Limits on the sensitivity of spherical gravitational wave detectors and on the accuracy of reconstructed signals

Thomas R. Stevenson*
Department of Physics, University of Maryland, College Park, Maryland 20742
(Received 15 November 1996)

A spherical geometry for a resonant-mass gravitational wave antenna offers significant improvements over traditional cylindrical antennas. However, completing a detector requires breaking the bare antenna's spherical symmetry by attaching multiple mechanical resonators and transducers. To fully assess the merits of such detectors, it is essential to be able to calculate the detector's sensitivity and the accuracy of the extractable signal information without relying on exact mathematical transducer or resonator symmetries to simplify the analysis, as has been done in previous work. Without making such assumptions, this paper generalizes the fundamental sensitivity limits, known for cylindrical detectors, that arise from the back-action noise present in any linear amplifier, and from thermal Brownian motion noise when detection bandwidth is limited. Optimal signal detection and estimation methods are derived by generalizing techniques used for one-dimensional detectors to the case of multiple interacting transducers. Formulas for the optimized signal-to-noise ratio are derived which generalize the connection between bandwidth and sensitivity known for one-dimensional detectors. A demand for isotropic sensitivity then gives requirements on transducer placement and matching. Comparing bandwidth anisotropies, the detector design proposed by Johnson and Merkowitz is found to be superior to an alternative proposal by Lobo and Serrano, and to be reasonably robust against asymmetries. In addition to sensitivity limits and optimal data analysis methods, limits are derived for the accuracy of reconstructed signal parameters such as direction, polarization, phase, and arrival time. [S0556-2821(97)01614-7]

PACS number(s): 04.80.Nn, 95.55.Ym

I. INTRODUCTION

To open up the era of gravitational wave astronomy, gravitational wave detectors must have both sufficient sensitivity to detect actual signals and the ability to extract as much signal information as possible. The use of spherical geometry for resonant-mass gravitational wave antennas offers a number of advantages over the traditional cylindrical bar shape in both these respects. The advantages are so compelling that construction of a new generation of resonant-mass spherical detectors is being proposed by a number of experimental groups [1] with the goal of operating concurrently with the first laser interferometers now under construction [2–4] and providing complementary information. However, analysis of the sensitivity and direction-finding accuracy of a spherical detector involves a number of complications, compared to the analysis of cylindrical detectors, which must be addressed before optimized detectors can be built with confidence.

Although a spherical antenna's enhanced gravitational cross section, its isotropic response and its ability to measure signal direction and polarization were recognized decades ago [5–7], building a practical detector requires breaking the spherical symmetry by attaching at least five additional mechanical resonators to readout the sphere's motion. In general, isotropic sensitivity is then lost and one has a rather complicated readout and signal reconstruction problem involving multiple transducer signals with correlated noise and complicated frequency response functions. This may have been one of the reasons why the benefits of using a spherical antenna were not pursued until Johnson and Merkowitz [8] showed that it is possible to locate six identical, radial transducers in positions with a special symmetry so that the readout problem is greatly simplified. Zhou and Michelson [9] then found an alternative set of five transducer locations which results in even greater conceptual simplification. However, any realistic experimental effort will not be able to guarantee completely identical transducers or positioning to arbitrary precision. Understanding how symmetric is symmetric enough for the transducers is an important question for the experimental groups now beginning to design spherical resonant-mass detectors [1] with the potential to detect a variety of realistic target sources [10,11]. This paper provides a rigorous analysis of the effects of transducer asymmetries on the capabilities of such detectors.

Previous work on this problem has provided only partial answers. In Johnson and Merkowitz's ground-breaking work [8,12], they derived equations of motion for five degenerate quadrupole spheroidal modes coupled to N identical, radial, single-mode, resonant transducers located at arbitrary points on the sphere's surface. Since for bar antennas the frequency splitting between the coupled antenna and transducer modes is an important measure of coupling which must be optimized, they conjectured an optimal design might correspond to one in which all mode splittings were equal. They found that for $N=5$ there apparently is no such configuration, while for $N=6$, placing the transducers at the centers of half the faces of a regular dodecahedron gives a spectrum with two degenerate quintuplets and a singlet. For that special set of transducer locations, Johnson and Merkowitz found (i) that they could simplify the equations of motion to obtain an analytical solution, (ii) by forming linear combinations of

*Electronic address: ts88@umail.umd.edu

transducer outputs, one could form ''mode channels,'' each of which coupled to one and only one of the five quadrupole components of the gravitational wave field thereby solving the signal deconvolution problem, and (iii) the frequency response for each mode channel was the same and had the same form as for a bar antenna with a single transducer. By numerical integration, they were then able to compute the sensitivity of such a detector. They made no effort to prove their arrangement was optimal, but they conjectured that detector sensitivity changes would be of second order in small departures from perfect dodecahedral symmetry and perfect transducer matching. As will be shown here, this is not completely correct. Also, Johnson and Merkowitz did not emphasize the importance of assuming that the transducers are identical not only in the mechanical parameters of their resonators, but also with respect to the magnitudes of the noise sources in each transducer. Only then are Johnson-Merkowitz mode channels statistically independent; if not, the sensitivity analysis needs modification. A third limitation is that Johnson and Merkowitz did not explicitly characterize the parameters of the equivalent bar detector which gives the same frequency response and noise spectrum as each of the mode channels.

The concepts of statistically independent transducer channels and effective antenna mass played a central role in the Zhou-Michelson analysis [9]. By using a combination of one radial and four tangential transducers located in a specific way, they demonstrated a different way of obtaining statistically independent transducer channels. With their proposed configuration, no linear combinations of transducer outputs need be formed: each transducer couples to only one quadrupole antenna mode, and consequently the detector's response to a gravitational wave is manifestly equivalent to attaching each transducer to a single-mode bar antenna, and since the transducer's back-action noise drives only its corresponding antenna mode, the transducer outputs are statistically independent. Zhou and Michelson calculated the effective antenna masses felt by each transducer and found different values for the radial and tangential transducers. Therefore, to make each independent channel have an identical frequency response, one would have to choose different parameters for each transducer. However, if each transducer had the same noise temperature T_n, and if thermal noise was negligible, they proved that the total signal-to-noise ratio (SNR) for detecting a known signal, using an optimal linear filter to combine the transducer outputs, is simply the energy E that an impulsive signal would deposit in an antenna initially at rest, divided by $k_B T_n$, independent of source direction and polarization. This generalized Giffard's amplifier limit for the sensitivity of bar antennas [13] to a spherical detector using the proposed transducer configuration. Zhou and Michelson also analyzed the accuracy of maximum likelihood estimates of the source direction and polarization using such a transducer configuration.

This paper extends the analysis of Johnson and Merkowitz, and Zhou and Michelson, by generalizing optimal linear filtering, and signal detection and estimation theory, for a detector with vector output rather than a scalar output. The generalized equations are written in a matrix notation designed not only to give a simple, compact, and intuitive notation, but also to clarify the connection between the signal-to-noise ratio theory for a spherical detector and that developed for bar antennas [13–15].

This approach leads to a variety of powerful results. First, it explicitly shows how to form statistically independent output channels, even in the absence of symmetries, which generalize the Johnson-Merkowitz mode channels or the Zhou-Michelson independent transducers. Second, it allows Price's method [15] for proving Giffard's amplifier limit [13] to be applied to a general linear detector with multiple transducers to yield a generalized theorem valid in particular for a spherical detector which lacks any special symmetries. Third, it yields formulas generalizing Price's high-Q expansion [15,11] of the detector's energy sensitivity. The high-Q expansion simplifies the discussion of the effects of asymmetries on detector performance, since particular values of temperature and antenna Q need not be assumed—rather the performance is characterized by the effective noise temperature in the lossless limit together with an effective bandwidth which characterizes the degradation of sensitivity with increasing thermal noise in the antenna. With the symmetries assumed by Johnson and Merkowitz, or Zhou and Michelson, the effective noise temperature and the effective bandwidth are independent of source direction and polarization, but detector asymmetries produce anisotropies in these quantities. This paper includes a numerical study of the size of those anisotropies in order to evaluate the tolerances required when designing a detector with the Johnson-Merkowitz proposed dodecahedral symmetry. SNR anisotropy is also used to compare the merits of the dodecahedral arrangement with other alternatives. A fourth product of the general theory is a set of analytical formulas giving the uncertainties in maximum likelihood estimates of the signal parameters in the limit of high SNR. The formulas are applied first to reproduce the Zhou-Michelson analytical and Monte Carlo results for their special design, and then they are used to investigate the effects of breaking the symmetry with nonidentical transducer noise temperatures.

Some of the results described here were presented briefly in two earlier papers [16,17], but the present paper offers a more detailed explanation and extends and applies the methods in new ways. Merkowitz and Johnson have carried their work further by constructing a prototype truncated icosahedral (TI) antenna instrumented with simple room-temperature nonresonant and resonant transducers [18,19]. With their prototype, they have experimentally investigated the effects of imperfect spherical symmetry in the *antenna*. Their results and this paper are complementary as the focus here is on asymmetries in the *transducer* locations and parameters. Lobo and Serrano [20] have recently published an analysis of the resonant mode splitting and transfer functions for N radial transducers mounted on a spherical antenna. They limited their analysis to identical transducers, and they did not consider noise, but based on their analysis they suggested an alternative way to locate transducers which is evaluated here based on its SNR anisotropy.

The first half of this paper gives an overview of the mathematics needed to calculate the SNR for a spherical gravitational wave detector with arbitrary transducer locations and parameters. In particular, Sec. II explains why the optimal strategy for detecting a known signal with a general linear detector with *vector* output is to perform an optimal linear

filtering operation which produces a *scalar* output with maximal SNR. An explicit matrix formula for the optimal linear filter is derived and compared with the well-known scalar formula. It is shown that by linear operations one can always form a set of *statistically independent* output channels, in terms of which the maximal SNR can be expressed very simply. Then a generalization of Giffard's theorem is proved in which the SNR for a lossless detector is related to the signal energy and the noise temperatures of the N transducers. Section III details how multidimensional optimal linear filtering and a matrix description of spherical detector dynamics combine to give general formulas for the SNR and its high-Q expansion in terms of an effective pulse detection noise temperature T_n^{eff} and effective fractional bandwidth δ^{eff}. After reviewing the effects of transducer symmetries in Sec. IV, the main focus in the second half of the paper is a numerical investigation of the effects of breaking those symmetries. Section V examines the effects of variations in the location, tuning, and noise temperatures of the transducers on T_n^{eff} and δ^{eff}. In Sec. VI, calculations of SNR anisotropy are used to evaluate the merits of alternative transducer locations, such as proposed by Lobo and Serrano [20], and to examine the robustness of the regular dodecahedral arrangement under a failure of one transducer. Section VII shows how the vector optimal filtering theory developed here can be used to analytically evaluate the uncertainties in maximum likelihood estimates of signal parameters such as amplitude, direction, polarization, arrival time, and phase. The theory is first applied to reproduce and extend the Zhou-Michelson results for their special transducer arrangement [9], and then the effects of some transducer asymmetries are numerically investigated. Finally, Sec. VIII summarizes the results.

II. MULTIDIMENSIONAL OPTIMAL LINEAR FILTERING

Suppose a general detector has a vector output $\mathbf{x}(t)$ consisting of N real functions of time:

$$\mathbf{x}(t)=(x_1(t),\ldots,x_N(t)), \tag{1}$$

and assume that a particular signal, if it is present, is known to give an output $\mathbf{x}=\mathbf{x}_{\text{sig}}$ in the absence of noise, but that the actual output is a linear superposition of the signal and noise processes. The *signal detection problem* is a case of hypothesis testing: decide, in an optimal way according to some reasonable criterion, whether or not the signal is in fact present. For a cylindrical gravitational wave detector with one transducer output, $N=1$, and one may draw on an extensive body of hypothesis-testing and signal detection and estimation theory which was largely developed in the effort to optimally design radar receivers [21–23].

For a spherical antenna instrumented with multiple transducers, $N>1$, and the question arises: is the theory for detector with vector output different from that for one with scalar output, and if so, how? It seems that the generalization of the theory to $N>1$ does not appear explicitly in the literature, at least not in the form needed for the analysis presented here. Hence, this section develops the answer. In fact, at three different levels three different answers are provided. First, on an abstract level, it is shown that there really is no difference: independent of N, a variety of different hypothesis testing criteria all lead to a decision rule based on optimal linear filtering to maximize the SNR. Second, on a more constructive level, generalized formulas are derived for the optimal filter and the resulting SNR which *are* different from the $N=1$ case, but which have a very similar form to the scalar formulas when written in matrix notation. Third, more substantive differences are shown to appear when one considers the limitations on detector sensitivity arising from back action of multiple transducer noise sources on the antenna.

The material in this section provides not only justification for the methods used in Secs. III–VI to investigate a spherical detector's SNR anisotropy, but also a foundation for further theoretical development in Sec. VII when the accuracy of signal parameter estimation is discussed. In addition, this section contains the most general results of this paper, results applicable to any linear detector without assuming spherical symmetry, particular transducer orientations, or other symmetries.

A. Signal detection and hypothesis testing

First, this section presents the abstract argument that the cases $N>1$ and $N=1$ are essentially the same. For both cases, the signal detection problem involves deciding between the hypothesis H_0 that the output is only noise and hypothesis H_1 that the output is noise plus the known signal. There are a variety of reasonable criteria one could use to make an ''optimal'' decision. For example, one could choose H_0 or H_1 based on which is most likely given the observed data, one could try to minimize the probability of making an error, one could assign costs to the different types of errors and try to minimize the expected cost (Bayes criterion), or one could maximize the detection probability for a fixed false alarm probability (Neyman-Pearson criterion). The theory of hypothesis testing (see Chap. 5 of [23]) says that all of these criteria are equivalent to the ''likelihood ratio test:''

$$\text{choose } H_1 \quad \text{if } \lambda\geqslant\lambda_0, \tag{2}$$

where the likelihood ratio

$$\lambda=\frac{P_1(\mathbf{x})}{P_0(\mathbf{x})} \tag{3}$$

is the ratio of the conditional probabilities of observing $\mathbf{x}$ given H_1 or H_0, and λ_0 is some threshold.

If the noise in the detector is Gaussian and stationary, then λ can be evaluated and a connection made with linear filtering as follows. Let $x_j(t_k)$ be samples of the data at a large number of times t_k. Although those samples likely have correlated noise, a linear transformation can be made to produce uncorrelated ''samples'' y_i [23]. Then

$$P_1(\mathbf{x})=\prod_i \frac{\Delta y_i}{\sqrt{2\pi}\sigma_i}\exp\left[\frac{-(y_i-y_i^{\text{sig}})^2}{2\sigma_i^2}\right], \tag{4}$$

where σ_i^2 is the variance of y_i and $y_i^{\rm sig}$ is the expected value of y_i if the signal is present. If H_0 is true, then P_0 is given by a similar formula with $y_i^{\rm sig}$ set to zero. The log-likelihood ratio is then found to be

$$\ln\lambda = \sum_i \left[y_i^{\rm sig} y_i - \frac{1}{2}(y_i^{\rm sig})^2 \right] \Big/ \sigma_i^2 \tag{5}$$

and the optimal decision rule is choose H_1 if

$$\sum_i y_i y_i^{\rm sig}/\sigma_i^2 \geqslant \ln\lambda_0 + \frac{1}{2}\sum_i (y_i^{\rm sig})^2/\sigma_i^2 . \tag{6}$$

The left-hand side of the above inequality is the value of the linear filter ν,

$$\nu = \sum_i a_i y_i , \tag{7}$$

which maximizes the energy SNR defined by

$$S/N = \frac{\nu_{\rm sig}^2}{\langle \nu_n^2 \rangle}. \tag{8}$$

Here $\nu_{\rm sig}$ is the filter output value for a noiseless signal, while $\langle \nu_n^2 \rangle$ is the variance of the output if there is only noise. As shown for example in [9], choosing filter coefficients proportional to

$$a_i = y_i^{\rm sig}/\sigma_i^2 \tag{9}$$

gives a maximal SNR of

$$S/N = \sum_i (y_i^{\rm sig})^2/\sigma_i^2 \tag{10}$$

and the decision rule is simply choose H_1 if the optimal linear filter output ν exceeds some threshold.

The value of N does not appear in the above argument reducing the signal detection problem to optimal linear filtering. Thus for detectors with either scalar or vector output, the optimal strategy for detecting a known signal is generally to compute the value of the optimal linear filter with *scalar* output ν which maximizes the SNR. If ν passes above some threshold, then a detection is claimed. This justifies the emphasis given the SNR in Secs. III–VI. Section VII uses the connection between the log-likelihood ratio and the optimal filter, given by Eq. (5), to analyze the accuracy with which unknown signal parameters may be estimated. First, however, rather than appealing abstractly to the existence of uncorrelated samples y_i, a more explicit formula for the optimal linear filter is needed in order to proceed further.

B. Explicit formula for the optimal filter

A practical formula for evaluating the optimal filter can be derived without having to compute uncorrelated samples y_i. In general, a linear filtering operation can be described in the Fourier domain by

$$\nu(\omega) = \mathbf{k}^\dagger(\omega)\mathbf{x}(\omega), \tag{11}$$

where $\mathbf{k}$ is a vector transfer function. From the abstract arguments above, the problem is how to do the filtering so as to maximize (at some instant of time t_0) the SNR defined by

$$S/N = |\nu_s(t_0)|^2/\langle \nu_n^2 \rangle, \tag{12}$$

where ν_s is the scalar output produced by the signal without noise and ν_n is the output produced by the noise.

The noise in the detector can be characterized by observing the noisy detector output in the absence of any signals and experimentally measuring the spectral density matrix $\mathbf{S}_x$ whose mnth component

$$S_x^{mn}(\omega) = \int_{-\infty}^{+\infty} e^{-j\omega\tau} \langle x_m(t) x_n(t-\tau) \rangle d\tau \tag{13}$$

is the Fourier transform of the correlation function for the mth and nth outputs. Then the signal and the noise factors in Eq. (12) are

$$\nu_s(t_0) = \int_{-\infty}^{+\infty} \frac{d\omega}{2\pi} e^{j\omega t_0} \mathbf{k}^\dagger(\omega)\mathbf{x}_{\rm sig}(\omega), \tag{14}$$

$$\langle \nu_n^2 \rangle = \int_{-\infty}^{+\infty} \frac{d\omega}{2\pi} \mathbf{k}^\dagger(\omega)\mathbf{S}_x(\omega)\mathbf{k}(\omega). \tag{15}$$

Using the calculus of variations to solve $\delta(S/N)/\delta k_i(\omega) = 0$ [24], one finds that choosing

$$\mathbf{k}^\dagger(\omega) = \mathbf{x}_{\rm sig}^\dagger(\omega)\mathbf{S}_x^{-1}(\omega) \tag{16}$$

maximizes the SNR (at $t_0 = 0$ for convenience), and that the value of the optimal SNR reduces from the ratio of two integrals to a single integral

$$S/N = \int_{-\infty}^{+\infty} \sigma(\omega) \frac{d\omega}{2\pi}, \tag{17}$$

where the integrand,

$$\sigma(\omega) = \mathbf{x}_{\rm sig}^\dagger(\omega)\mathbf{S}_x^{-1}(\omega)\mathbf{x}_{\rm sig}(\omega), \tag{18}$$

gives the available SNR density per unit bandwidth. For $N = 1$, Eq. (16) and Eq. (18) reduce to the well-known result [23,25] for detectors with scalar output: the optimal filter transfer function is the conjugate of the Fourier transform of the signal divided by the noise spectral density and $\sigma(\omega)$ is the absolute square of the signal spectrum divided by the noise spectral density. In the vector case the formulas *are* somewhat different since matrix inversion of $\mathbf{S}_x$ is involved, and the factors do not commute, but in matrix notation the formulas are no more complicated than in the scalar case.

While uncorrelated samples y_i were not needed above to compute the optimal filter, it is easy to show explicitly how to construct linear combinations of the transducer outputs $x_m(t)$ which are statistically independent. Inspection of the definition of $\mathbf{S}_x(\omega)$ in Eq. (13) shows that $\mathbf{S}_x(\omega)$ is an $N \times N$ Hermitian matrix,

$$\mathbf{S}_x = \mathbf{S}_x^\dagger , \tag{19}$$

and hence it can be diagonalized by a unitary matrix $\mathbf{U}(\omega)$. A new vector output $\mathbf{y}$ defined by

$$\mathbf{y}(\omega)=\mathbf{U}^{\dagger}(\omega)\mathbf{x}(\omega) \tag{20}$$

then has a spectral density matrix

$$\mathbf{S}_y=\mathbf{U}^{\dagger}\mathbf{S}_x\mathbf{U} \tag{21}$$

$$=\mathrm{diag}(\zeta_1(\omega),\ldots,\zeta_N(\omega)). \tag{22}$$

Each new output channel $y_i(t)$ is statistically independent from the others, and it has a noise spectral density $\zeta_i(\omega)$ which is an eigenvalue of $\mathbf{S}_x$. One finds the total optimal SNR given by Eqs. (17) and (18) is the sum of the available SNR in each statistically independent output channel:

$$S/N=\sum_{i=1}^{N}\frac{[y_i^{\mathrm{sig}}(t)]^2}{\langle y_i^2\rangle} \tag{23}$$

$$=\sum_{i=1}^{N}\int_{-\infty}^{+\infty}\frac{|y_i^{\mathrm{sig}}(\omega)|^2}{\zeta_i(\omega)}\frac{d\omega}{2\pi}. \tag{24}$$

C. Amplifier limit for $N>1$

Gravitational wave detectors look for such small signals that maximizing the SNR as far as fundamental limits allow is vital. Braginsky [26] was the first to recognize that the effect of amplifier noise on the antenna's motion must be considered in calculating the limit of sensitivity. Giffard [13] showed that, for a cylindrical antenna with a nonresonant transducer coupled to a linear amplifier, the SNR for detecting a burst signal approaches the limit

$$S/N=\frac{E}{k_BT_n} \tag{25}$$

as the thermal noise in the antenna is reduced to zero by lowering the physical temperature to zero or increasing its mechanical quality factor Q to infinity. Here E is the energy that the gravitational wave burst would deposit in an antenna initially at rest, and T_n is the noise temperature of the mechanical amplifier, defined by

$$k_BT_n=\sqrt{S_fS_u-[\mathrm{Im}(S_{fu})]^2}, \tag{26}$$

where S_f, S_u are respectively the spectral densities of the amplifier's back-action force noise and its additive velocity noise, and S_{fu} is the force-velocity cross-spectral density. (To avoid violating the Heisenberg uncertainty principle, $k_BT_n\geqslant\hbar\omega$ [27].) Michelson and Taber [14] proved that Eq. (25) is a general limit applying also for any lossless, passive, transducer.

For a detector with vector output, Eq. (25) needs to be generalized since there is in principle a different T_n for each of the N transducers. Below, Price's method [15] for proving Eq. (25) is used to derive a generalized theorem applicable to a spherical gravitational wave detector with arbitrary asymmetries.

Assuming that the detector is linear and thermal noise is negligible compared to back-action noise, the output of the detector can be written as

$$\mathbf{x}(\omega)=\mathbf{Y}_{ts}(\omega)\mathbf{f}_s(\omega)+\mathbf{Y}_{tt}(\omega)\mathbf{f}_t(\omega), \tag{27}$$

where $\mathbf{Y}_{ts}$ and $\mathbf{Y}_{tt}$ are matrices which describe respectively the response to signal forces $\mathbf{f}_s$ acting on the (''spherical'') antenna and the response to back-action forces $\mathbf{f}_t$ arising in the transducers. (Explicit formulas for $\mathbf{Y}_{ts}$ and $\mathbf{Y}_{tt}$ for a spherical antenna with radial transducers are derived in Sec. III below.) Let $\mathbf{s}_u$, $\mathbf{s}_f$, and $\mathbf{s}_{fu}$ be, respectively, vectors listing the velocity, force, and force-velocity noise spectral densities of the transducers. With the transducer output vector $\mathbf{x}$ calibrated, say, to measure the transducer velocities $\mathbf{u}_t$, the expected signal is

$$\mathbf{x}_{\mathrm{sig}}=\mathbf{Y}_{ts}\mathbf{f}_s, \tag{28}$$

and the detector's spectral density matrix is

$$\mathbf{S}_x=\mathrm{diag}(\mathbf{s}_u)+\mathbf{Y}_{tt}\mathrm{diag}(\mathbf{s}_{fu})+\mathrm{diag}(\mathbf{s}_{fu})^{\dagger}\mathbf{Y}_{tt}^{\dagger}+\mathbf{Y}_{tt}\mathrm{diag}(\mathbf{s}_f)\mathbf{Y}_{tt}^{\dagger}. \tag{29}$$

The signal-to-noise ratio density is then

$$\sigma(\omega)=\mathbf{f}_s^{\dagger}\mathbf{Y}_{ts}^{\dagger}\mathbf{S}_x^{-1}\mathbf{Y}_{ts}\mathbf{f}_s. \tag{30}$$

If the transducer systems are lossless and passive as is the antenna, then energy conservation implies the reciprocity relation $\mathbf{Y}_{tt}^{\dagger}=-\mathbf{Y}_{tt}$. For many amplifiers (including superconducting quantum interference device (SQUID) amplifiers coupled through lossless passive electromechanical transducers [28]), the time-reversal symmetries of the amplifier's equations of motion imply that $\mathbf{s}_{fu}$ is pure imaginary. With these two assumptions, the spectral density matrix can be written as

$$\mathbf{S}_x=\mathrm{diag}(\mathbf{s}_u)+j\mathbf{Y}_{tt}\mathrm{diag}[\mathrm{Im}(\mathbf{s}_{fu})]+\mathrm{diag}[\mathrm{Im}(\mathbf{s}_{fu})]j\mathbf{Y}_{tt}-\mathbf{Y}_{tt}\mathrm{diag}(\mathbf{s}_f)\mathbf{Y}_{tt}. \tag{31}$$

For the case $N=1$, Price [15] showed that there is an equivalent physical model for the behavior of $\sigma(\omega)$. He showed that $\sigma(\omega)=e(\omega)/k_BT_n$, where $e(\omega)$ is the spectrum of energy which would be dissipated if the signal force was applied to the lossless detector after replacing the amplifier by a mechanical impedance equal to its noise impedance Z_n defined by

$$Z_n=[k_BT_n+j\mathrm{Im}(S_{fu})]/S_u. \tag{32}$$

For the case $N>1$, suppose that each amplifier is replaced by its noise impedance. Then reaction forces $\mathbf{f}_t=-\mathrm{diag}(\mathbf{z}_n)\mathbf{u}_t$ appear in Eq. (27). The resulting transducer velocity response to the signal is $\mathbf{u}_t=\mathbf{v}$, with

$$\mathbf{v}=[\mathbf{I}+\mathbf{Y}_{tt}\mathrm{diag}(\mathbf{z}_n)]^{-1}\mathbf{Y}_{ts}\mathbf{f}_s, \tag{33}$$

where $\mathbf{I}$ is the identity matrix and $\mathbf{z}_n$ is the vector listing the noise impedance of each transducer. Then the spectrum of energy which would be dissipated in the noise impedances is

$$e(\omega)=\mathbf{v}^{\dagger}\mathrm{diag}[\mathrm{Re}(\mathbf{z}_n)]\mathbf{v}. \tag{34}$$

Using the relations between k_BT_n, Z_n, $\mathbf{s}_f$, $\mathbf{s}_u$, and $\mathbf{s}_{fu}$, together with the assumptions that $\mathbf{Y}_{tt}^{\dagger}=-\mathbf{Y}_{tt}$ and $\mathbf{s}_{fu}$ is pure

imaginary, the above expression for $e(\omega)$ can be expanded out and some terms canceled to give

$$e(\omega)=\mathbf{f}_s^\dagger \mathbf{Y}_{ts}^\dagger \mathbf{B}^{-1}\mathbf{Y}_{ts}\mathbf{f}_s, \tag{35}$$

where

$$\mathbf{B}=\mathrm{diag}\left(\frac{\mathbf{s}_u}{k_B\mathbf{T}_n}\right)+j\mathbf{Y}_{tt}\mathrm{diag}\left[\frac{\mathrm{Im}(\mathbf{s}_{fu})}{k_B\mathbf{T}_n}\right]+\mathrm{diag}\left[\frac{\mathrm{Im}(\mathbf{s}_{fu})}{k_B\mathbf{T}_n}\right]j\mathbf{Y}_{tt}$$
$$-\mathbf{Y}_{tt}\mathrm{diag}\left[\frac{\mathbf{s}_f}{k_B\mathbf{T}_n}\right]\mathbf{Y}_{tt}. \tag{36}$$

Comparison of Eqs. (30) and (31) with Eqs. (35) and (36) shows that $\sigma(\omega)$ and $e(\omega)$ have very similar forms. If the transducers all have identical noise temperatures, it is clear that $\sigma(\omega)=e(\omega)/k_BT_n$ just as for the case $N=1$.

If the transducer noise temperatures are not identical, then $\sigma(\omega)$ can still be put into a form analogous to Eq. (34):

$$\sigma(\omega)=\mathbf{v}^\dagger\mathbf{A}^{-1}\mathbf{v}, \tag{37}$$

where

$$\mathbf{A}=\mathrm{diag}\left[\frac{k_B\mathbf{T}_n}{\mathrm{Re}(\mathbf{z}_n)}\right]+[\mathbf{I}+\mathbf{Y}_{tt}\mathrm{diag}(\mathbf{z}_n)]^{-1}[\mathrm{diag}(k_B\mathbf{T}_n),\mathbf{Y}_{tt}]$$
$$\times\{[\mathbf{I}+\mathbf{Y}_{tt}\mathrm{diag}(\mathbf{z}_n)]^{-1}\}^\dagger. \tag{38}$$

The commutator in the second term of $\mathbf{A}$ above is zero when $\mathbf{Y}_{tt}$ is diagonal so that the transducers do not affect one another as in the Zhou-Michelson independent transducer scheme [9]. In that case,

$$\sigma(\omega)=\mathbf{v}^\dagger\mathrm{diag}\left[\frac{\mathrm{Re}(\mathbf{z}_n)}{k_B\mathbf{T}_n}\right]\mathbf{v}, \tag{39}$$

so that, for independent transducers, the SNR is the weighted sum of the energies dissipated in the noise impedances, each energy being divided by its corresponding noise temperature. Since each component of $\mathbf{T}_n$ and $\mathrm{Re}(\mathbf{z}_n)$ is positive, Eq. (39) and Eq. (34) imply that $\sigma(\omega)$ satisfies the inequalities

$$\frac{e(\omega)}{\max(k_B\mathbf{T}_n)}\leqslant\sigma(\omega)\leqslant\frac{e(\omega)}{\min(k_B\mathbf{T}_n)}. \tag{40}$$

Integrating over all frequencies gives

$$\frac{E}{\max(k_B\mathbf{T}_n)}\leqslant S/N\leqslant\frac{E}{\min(k_B\mathbf{T}_n)}, \tag{41}$$

where

$$E=\int_{-\infty}^{\infty}e(\omega)\frac{d\omega}{2\pi}. \tag{42}$$

Since the detector is assumed lossless, energy conservation implies that the total energy E dissipated in the noise impedances equals the total energy an impulsive signal would initially deposit in an antenna initially at rest irrespective of whether or not the amplifiers are replaced by their noise impedances.

The general case of interacting transducers, with $\mathbf{Y}_{tt}$ not diagonal, is more complicated since $\sigma(\omega)$ and $e(\omega)$ are not so closely related as in Price's equivalent model for the scalar case. However, numerical experiments show that the effect of the extra commutator term in Eq. (38) is always to shift the eigenvalues of $\mathbf{A}(\omega)$ closer to the average of $k_BT_n/\mathrm{Re}(Z_n)$ without changing the sum of the eigenvalues. Therefore, the inequalities in Eqs. (40) and (41) are valid for the general case also, as is verified by the numerical results of Sec. V C.

Equation (41) generalizes Giffard's amplifier limit theorem to a lossless linear detector with vector output having a range of amplifier noise temperatures. If all the noise temperatures are identical, then the lower and upper bounds on the SNR are both simply E/k_BT_n and the minimum detectable energy (for SNR=1) is k_BT_n. Of course, to attain this limiting sensitivity an experimenter has to fully characterize the detector by measuring $\mathbf{x}_{\mathrm{sig}}$ and $\mathbf{S}_x$ and then implement the optimal filter given by Eq. (16).

One might wonder why there seems to be no improvement in sensitivity if several identical transducers are placed close together on the antenna so that they essentially monitor the motion of the same point on the antenna and form a composite transducer. Even after averaging the outputs of the N transducers the minimum detectable energy is unchanged from the value k_BT_n which would be obtained if only one transducer were used. The explanation is that while the additive noise is reduced by averaging to $\mathbf{s}_u/N$, the total force noise for the composite transducer is increased to $N\mathbf{s}_f$, with $\mathbf{s}_{fu}$ and k_BT_n unchanged. However, the composite transducer does have an N times larger noise impedance which, as explained in Sec. III below, increases the detection bandwidth, and improves the sensitivity when the detector is not lossless and thermal noise is significant.

III. SPHERICAL DETECTOR DYNAMICS

While the preceding section considered the sensitivity of a general linear detector with vector output, the rest of this paper specializes to a spherical gravitational wave antenna with N transducer systems coupling only to radial motion. Perfect spherical symmetry (or at least degenerate quadrupole modes) is assumed, but the transducers may be located arbitrarily and may have completely different mechanical and noise parameters. Although the methods used below could be adapted to consider nonradial transducers as proposed by Zhou and Michelson [9], radial transducers were chosen for several reasons: (i) to provide the basis for a concrete analysis of possible detector behavior, (ii) most existing detectors use transducers monitoring motion normal to the antenna surface, and (iii) the Johnson-Merkowitz dodecahedral arrangement [8] employs identical radial transducers, which is a definite practical advantage over the Zhou-Michelson mix of radial and tangential transducers which require resonator masses differing by a factor of about 13 [9] to give matched responses.

The dynamics of a sphere interacting with radial transducers and gravitational waves is described below using matrices suited to evaluating the optimal filter and SNR. Antenna thermal noise is included, and a high-Q expansion derived

which forms the basis for analyzing the effects of transducer asymmetries.

A. Bare sphere

Before showing how matrix notation can be used to compactly describe the dynamics of a spherical gravitational wave antenna interacting with N resonant-mass transducer systems, consider the dynamics of a bare sphere. The velocity $\vec{u}_s$ of the sphere at position $\vec{r}$ can be written as a sum over normal modes:

$$\vec{u}_s(\vec{r},\omega)=\sum_n a_n(\omega)\vec{\phi}_n(\vec{r}), \tag{43}$$

where the $\vec{\phi}_n(\vec{r})$ are the orthogonal elastic eigenfunctions of the sphere.

When transducers are attached to the sphere, the values of $\vec{u}_s(\vec{r},\omega)$ at the attachment points will be of primary importance. So let

$$\mathbf{u}_s(\omega)=(\hat{r}_1\cdot\vec{u}_s(\vec{r}_1,\omega),\ldots,\hat{r}_N\cdot\vec{u}_s(\vec{r}_N,\omega)) \tag{44}$$

be the N-dimensional vector of radial sphere velocities at N locations $\vec{r}_a$ on the sphere's surface. Let $\mathbf{f}_s$ be a vector of N radial forces applied at the points $\vec{r}_a$. Then the response of the bare sphere can be described by a mechanical admittance matrix $\mathbf{Y}_0$ which gives the values of the sphere velocities as a linear response to the applied forces:

$$\mathbf{u}_s(\omega)=\mathbf{Y}_0(\omega)\mathbf{f}_s(\omega). \tag{45}$$

The general eigenmode expansion of the admittance matrix of a linear system gives the components of $\mathbf{Y}_0$ as

$$Y_0^{ab}=\sum_n \frac{1}{s+\omega_n^2/s+\omega_n/Q_n}\frac{[\hat{r}_a\cdot\vec{\phi}_n(\vec{r}_a)][\hat{r}_b\cdot\vec{\phi}_n(\vec{r}_b)]}{\int\rho(\vec{r})|\vec{\phi}_n(\vec{r})|^2d^3r}, \tag{46}$$

where ω_n and Q_n are the resonance frequency and quality factor of the nth mode, $s=j\omega$, and ρ is the density.

Equation (46) is nothing more than the result of applying the usual eigenfunction method of solving the elastic equations of motion, but with the normalization chosen to give admittance matrix elements. When Eq. (43) is substituted into the equations of motion, the denominator of Y_0^{ab} arises from multiplying the differential operator acting on $\vec{u}_s$ by $\vec{\phi}_n(\vec{r})$ and integrating over volume. The $\hat{r}_b\cdot\vec{\phi}_n(\vec{r}_b)$ factor in the numerator comes from the overlap integral between the point force applied at $\hat{r}_b$ and $\vec{\phi}_n(\vec{r})$, while the $\hat{r}_a\cdot\vec{\phi}_n(\vec{r}_a)$ factor comes from evaluating the solution for the velocity response at $\hat{r}_a$ in the radial direction. Spherical symmetry implies that the radial eigenfunctions $\hat{r}_a\cdot\vec{\phi}_n(\vec{r}_a)$ are proportional to the real spherical harmonics (see Sec. III D below).

For a gravitational wave antenna, the amplitudes of the five degenerate quadrupole spheroidal modes are of primary interest. At frequencies sufficiently near the lowest quadrupole frequency ω_0, the expansion for $\mathbf{Y}_0$ is dominated by the five terms with poles at $\pm\omega_0$. Keeping just those terms, one has the following simple form for $\mathbf{Y}_0$:

$$\mathbf{Y}_0\approx[\mu(s+\omega_0^2/s+\omega_0/Q_0)]^{-1}\mathbf{M}\quad\text{for}\quad\omega\approx\pm\omega_0, \tag{47}$$

where μ is the effective mass of the antenna and $\mathbf{M}$ is the matrix with elements

$$M_{ab}=(3\cos^2\theta_{ab}-1)/2, \tag{48}$$

where θ_{ab} is the angle between $\vec{r}_a$ and $\vec{r}_b$.

Mathematically, μ is one half the reciprocal of the residue of the radial driving point admittance of the sphere at $s=j\omega_0$. Physically, if the sphere is driven at ω_0 with a radial force at any single point, the ratio of energy stored in the motion of the sphere to squared radial velocity at that point is the same as if one was driving a mass μ attached to an infinite mass by a spring $\mu\omega_0^2$. The response of the sphere at locations other than the drive point is encoded by $\mathbf{M}$. Equation (48) can be derived from Eq. (46) using properties of the spherical harmonics for $\ell=2$, but the result can be inferred: in a coordinate system in which the drive point is at the north pole, the only quadrupole spherical harmonic excited is the one with $m=0$, which has the angular form appearing in Eq. (48).

For the fundamental quadrupole frequency of a sphere, Zhou and Michelson [9] evaluated μ as a function of the antenna material's Poisson ratio. For a Poisson ratio of 0.33, $\mu=0.302M_s$, where M_s is the total physical mass of the sphere. Interest has also been expressed in other sets of quadrupole modes for gravity wave detection, especially the next higher frequency group [29,30]. The radial eigenfunction for the second quadrupole modes nearly has a node at the sphere surface [31,6,29], so those modes do not couple as easily to surface mounted transducers as do the lowest modes. For the second quadrupole modes at the surface, this author calculates $\mu=455M_s$, but if holes were bored into the sphere so that radial transducers could be mounted at $r=0.46R_s$ at the antinode of the modes, then $\mu=0.281M_s$ is quite similar to the value for the fundamental quadrupole modes at the surface.

B. Sphere with N radial transducers

Armed with the admittance matrix $\mathbf{Y}_0$ for a bare sphere, it is relatively simple to describe the dynamics of the sphere when instrumented with N radial, resonant-mass transducer systems attached to its surface. The simplest such transducer systems would consist of a set of N masses attached to the sphere by springs with electromechanical amplifiers measuring the radial displacement of each mass relative to its attachment point on the sphere surface. (More complicated, multimode, transducer systems with several mass-spring stages chained together [32] can be handled similarly as is described later.)

If N single-mode transducer systems are used, let $\mathbf{m}_t$, $\mathbf{k}_t$, $\mathbf{u}_t$, and $\mathbf{f}_t$ be, respectively, N-vectors listing the transducer masses, the transducer springs, and the relative velocities and external forces applied between the transducer masses and their attachment points. Then the dynamics of the detector is described by

$$\begin{bmatrix} \mathbf{u}_s \\ \mathbf{u}_t \end{bmatrix} = \mathbf{Y} \begin{bmatrix} \mathbf{f}_s \\ \mathbf{f}_t \end{bmatrix}, \tag{49}$$

where the grand admittance matrix $\mathbf{Y}$ is a $2N \times 2N$ matrix comprised of four $N \times N$ submatrices $\mathbf{Y}_{ss}$, $\mathbf{Y}_{st}$, $\mathbf{Y}_{ts}$, $\mathbf{Y}_{tt}$:

$$\mathbf{Y} = \begin{bmatrix} \mathbf{Y}_{ss} & \mathbf{Y}_{st} \\ \mathbf{Y}_{ts} & \mathbf{Y}_{tt} \end{bmatrix} \tag{50a}$$

$$= \begin{bmatrix} \mathbf{Y}_0^{-1} + \mathrm{diag}(\mathbf{m}_t s) & \mathrm{diag}(\mathbf{m}_t s) \\ \mathrm{diag}(\mathbf{m}_t s) & \mathrm{diag}(\mathbf{k}_t / s + \mathbf{m}_t s) \end{bmatrix}^{-1}. \tag{50b}$$

As Eq. (50b) indicates, the detector's impedance matrix $\mathbf{Z} = \mathbf{Y}^{-1}$ is given by the composite impedance matrix describing N isolated transducer systems, but with the bare sphere's impedance matrix $\mathbf{Y}_0^{-1}$ added to the sphere-sphere submatrix. This simply states that, if the velocities of the transducer masses and the sphere attachment points are specified, the required forces are the forces needed to make isolated transducer systems move as prescribed, plus extra forces on the transducer attachment points equal to the forces needed to move the bare sphere to follow the attachment points.

For the case of multimode transducer systems, the generalization of Eq. (50b) uses the impedance matrix elements for chains of mass-spring stages, which, although more complicated, can be readily calculated using partial fraction techniques [33]. For example, for a two-mode transducer system with final masses and springs m_2, k_2 and intermediate masses and springs m_1, k_1 the transducer impedance matrix for the isolated system is

$$\left\{ \left(\begin{bmatrix} m_2 s & m_2 s \\ m_2 s & m_2 s + \dfrac{k_2}{s} \end{bmatrix} + \begin{bmatrix} m_1 s & 0 \\ 0 & 0 \end{bmatrix} \right)^{-1} + \begin{bmatrix} \dfrac{s}{k_1} & 0 \\ 0 & 0 \end{bmatrix} \right\}^{-1}. \tag{51}$$

C. Spectral density matrix

The transducers which measure $\mathbf{u}_t$ can be characterized as electromechanical amplifiers with additive velocity noise spectral densities $\mathbf{s}_u$, producing back-action noise forces $\mathbf{f}_t$ with spectral densities $\mathbf{s}_f$. Correlation between the force and velocity noise of each amplifier is described by the cross-spectral densities $\mathbf{s}_{fu}$. Then the cross-spectral density matrix appearing in Eq. (13) is

$$\mathbf{S}_x = \mathrm{diag}(\mathbf{s}_u) + \mathbf{Y}_{tt}\mathrm{diag}(\mathbf{s}_{fu}) + \mathrm{diag}(\mathbf{s}_{fu})^{\dagger}\mathbf{Y}_{tt}^{\dagger} + \mathbf{Y}_{tt}\mathrm{diag}(\mathbf{s}_f)\mathbf{Y}_{tt}^{\dagger} + 2k_B T\ \mathrm{Re}(\mathbf{Y}_{tt}), \tag{52}$$

where the term proportional to the real part of $\mathbf{Y}_{tt}$ gives the thermal noise required by the fluctuation-dissipation theorem [34] for a detector at temperature T.

If all five of the antenna's quadrupole modes have the same quality factor Q_0, as assumed in Eq. (47), then expanding Eq. (50b) to first order in Q_0^{-1}, one finds [35]

$$\mathrm{Re}(\mathbf{Y}_{tt}) = (\mu\omega_0 / Q_0)\mathbf{Y}_{ts}\mathbf{M}^{-1}\mathbf{Y}_{ts}^{\dagger}. \tag{53}$$

D. Interaction with a gravitational wave

The radial motion of the bare sphere's quadrupole modes is given by the five real spherical harmonics ψ_n for $\ell = 2$,

$$\begin{bmatrix} \psi_0 \\ \psi_c \\ \psi_s \\ \psi_{2c} \\ \psi_{2s} \end{bmatrix} = \sqrt{\frac{5}{16\pi}} \begin{bmatrix} 3\cos^2\theta - 1 \\ -\sqrt{3}\cos\phi\sin 2\theta \\ -\sqrt{3}\sin\phi\sin 2\theta \\ \sqrt{3}\cos 2\phi\sin^2\theta \\ \sqrt{3}\sin 2\phi\sin^2\theta \end{bmatrix} \tag{54a}$$

$$= \sqrt{\frac{5}{16\pi}} \begin{bmatrix} 3z^2/r^2 - 1 \\ -2xz/r^2 \\ -2yz/r^2 \\ (x^2 - y^2)/r^2 \\ 2xy/r^2 \end{bmatrix}. \tag{54b}$$

Assuming that general relativity correctly describes the interaction, a plane gravitational wave excites only the ψ_{2c} and ψ_{2s} modes in a coordinate system with the wave traveling down the z axis. More general metric gravitational theories can produce a different interaction [29], but in this paper general relativity will be assumed to hold. In the wave-directed frame, the overlap integrals of the gravitational tidal forces with the sphere modes are [9]

$$\mathbf{f}'_m = (\omega/\omega_0)^2 \sqrt{\Pi \pi \rho v_s^5 f_0^{-1}}\,(0,0,0,h_+(\omega), -h_\times(\omega)), \tag{55}$$

where $h_+(\omega)$ and $h_\times(\omega)$ are the Fourier amplitudes of the two polarization components of the wave, ρ and v_s are, respectively, the density and extensional sound velocity of the antenna material, and $\Pi \approx 0.201$ is the reduced energy cross section of the spherical antenna. The expression for $\mathbf{f}'_m$ is normalized so that

$$E = \frac{1}{2}[\mathbf{f}'_m(\omega_0)]^{\dagger}\mathbf{f}'_m(\omega_0) \tag{56}$$

is the energy deposited in the antenna. If coordinates $\vec{r}'$ in the wave frame are related to detector coordinates $\vec{r}$ by a rotation matrix $\mathbf{R}$,

$$\vec{r}' = \mathbf{R}(\phi_{\mathrm{gw}}, \theta_{\mathrm{gw}}, \psi_{\mathrm{gw}})\vec{r}, \tag{57}$$

with Euler angles ϕ_{gw}, θ_{gw}, and ψ_{gw}, then the force overlap components in the detector frame are given by a transformation law,

$$\sum_n f_m^n \psi_n(\vec{r}) = \sum_n f_m'^n \psi_n(\mathbf{R}\vec{r}), \tag{58}$$

which is well known for the spherical harmonics [9]. With the sign conventions chosen in Eq. (54a), the transformation law is

$$\mathbf{f}_m=(\omega/\omega_0)^2\sqrt{\Pi\pi\rho v_s^5 f_0^{-1}}$$

$$\times\begin{bmatrix}\frac{\sqrt{3}}{2}\sin^2\theta h_+\\ \frac{1}{2}\sin 2\theta\cos\phi h_+ + \sin\theta\sin\phi h_\times\\ \frac{1}{2}\sin 2\theta\sin\phi h_+ - \sin\theta\cos\phi h_\times\\ \frac{1}{2}(1+\cos^2\theta)\cos 2\phi h_+ + \cos\theta\sin 2\phi h_\times\\ \frac{1}{2}(1+\cos^2\theta)\sin 2\phi h_+ - \cos\theta\cos 2\phi h_\times\end{bmatrix}, \quad (59)$$

provided a detector coordinate convention is chosen so that $\psi_{\rm gw}=0$.

If $N\geqslant 5$, then there are sufficient degrees of freedom (provided no two transducers have the same or antipodal attachment points) to excite any linear combination of the five quadrupole modes using the point forces $\mathbf{f}_s$. Therefore, the description of the detector dynamics derived above can be used to model the detector interaction with a gravitational wave by finding point forces which mimic the effects of the distributed gravitational forces on the antenna. (The gravitational forces on the transducer masses are neglected because of their much smaller size compared to the sphere.) The required equation for $\mathbf{f}_s$ is

$$\mathbf{f}_m=\sqrt{4\pi/5\mu}\,\mathbf{G}^T\mathbf{f}_s, \quad (60)$$

where the $N\times 5$ matrix $\mathbf{G}$ has components

$$G_{an}=\psi_n(\hat{r}_a). \quad (61)$$

If $N\geqslant 6$, then solutions for $\mathbf{f}_s$ are not unique. Any solution to Eq. (60) gives a valid description of the detector response; for definiteness and numerical stability, the pseudoinverse [36] of $\mathbf{G}^T$ was used to solve Eq. (60).

Apart from different normalization, the matrix $\mathbf{G}^T$ is the same as the ''pattern matrix'' defined by Johnson and Merkowitz [8], and is related to $\mathbf{M}$ by

$$\mathbf{M}=\frac{4\pi}{5}\mathbf{G}\mathbf{G}^T. \quad (62)$$

E. SNR and high Q expansion

All the ingredients needed to compute the SNR for a spherical gravitational wave detector using the general formulas of Sec. II are now in place. According to Eq. (49), the N transducers give a vector output $\mathbf{x}_{\rm sig}=\mathbf{Y}_{ts}\mathbf{f}_s$, where $\mathbf{f}_s$ is a solution of Eq. (60). With $\mathbf{S}_x$ given by Eq. (52), Eq. (18) for the signal-to-noise density becomes

$$\sigma(\omega)=\mathbf{f}_s^\dagger\mathbf{K}(\omega)\mathbf{f}_s, \quad (63)$$

where

$$\mathbf{K}(\omega)=\mathbf{Y}_{ts}^\dagger[\mathbf{S}_x(\omega)]^{-1}\mathbf{Y}_{ts}. \quad (64)$$

For a given set of detector parameter values, $\mathbf{K}(\omega)$ can be computed; for given source direction and polarization amplitudes, a value for $\mathbf{f}_s$ can be found, then Eq. (63) allows $\sigma(\omega)$ to be evaluated; finally, numerical integration gives the value of the SNR. However, before launching into a numerical study of how the SNR behaves, it is desirable to have a deeper analytical understanding of how the SNR depends on the signal wave form and on the detector design. Much theoretical insight can be gained in this regard by drawing parallels with the theory developed for resonant-bar detectors.

The performance of bar detectors is often characterized by their sensitivity to impulsive burst signals which have Fourier components which vary little over the detection bandwidth where $\sigma(\omega)$ is large. For impulsive signals, the SNR is proportional to the energy E that the signal would deposit in the antenna if it were initially at rest. The pulse detection noise temperature T_p is then defined as

$$k_BT_p\equiv\frac{E}{S/N}. \quad (65)$$

While E for a bar-antenna depends on source direction and polarization, T_p does not. As described in Sec. II C, Giffard [13] showed that T_p approaches the amplifier's noise temperature T_n [defined by Eq. (26)] in the limit that the mechanical Q's approach infinity. For high but finite Q's, T_p exceeds T_n by a sum of terms of order $k_BT/(Q_i\delta)$, where Q_i is the Q of the ith resonator in an antenna-multimode-resonator chain and δ is the fractional bandwidth shown by $\sigma(\omega)$ for a given detector design. Price [15] explored the sensitivity of T_p to dissipation as the basis of optimal detector design: in the ''lossless limit,'' any choice of transducer masses and springs gives $T_p=T_n$, but in the presence of dissipation, it is best to choose masses and springs in a clever way to make the detector as ''loss tolerant'' as possible. Price found that typically the sensitivity to antenna dissipation was as great as the dissipation in any of the transducer resonators. His work leads to a natural, precise, definition for δ [11] which characterizes the sensitivity to the antenna Q_0, and he showed how to choose masses and springs to make δ large by making $\sigma(\omega)$ ''maximally flat.''

How does the theory for bar detectors carry over to spheres? Equations (52) and (53), and (63) and (64) hold the answer. Defining the pulse detection noise temperature as for bars, and then expanding to first order in T/Q_0, one finds

$$k_BT_p(\mathbf{f}_s)\equiv\frac{E}{S/N} \quad (66a)$$

$$\approx k_BT_n^{\rm eff}(\mathbf{f}_s)+\frac{k_BT}{Q_0}\frac{\pi}{\delta^{\rm eff}(\mathbf{f}_s)}, \quad (66b)$$

where

$$k_BT_n^{\rm eff}(\mathbf{f}_s)=\frac{\mathbf{f}_s^\dagger[(1/2\mu)\mathbf{M}]\mathbf{f}_s}{\mathbf{f}_s^\dagger[\int_{-\infty}^{+\infty}\mathbf{K}_0(\omega)d\omega/2\pi]\mathbf{f}_s} \quad (67)$$

and

$$\delta^{\rm eff}(\mathbf{f}_s)=\frac{(\pi/\omega_0)[\mathbf{f}_s^\dagger[\int_{-\infty}^{+\infty}\mathbf{K}_0(\omega)d\omega/2\pi]\mathbf{f}_s]^2}{\mathbf{f}_s^\dagger\mathbf{M}\mathbf{f}_s\mathbf{f}_s^\dagger[\int_{-\infty}^{+\infty}\mathbf{K}_0(\omega)\mathbf{M}^{-1}\mathbf{K}_0(\omega)d\omega/2\pi]\mathbf{f}_s}. \quad (68)$$

For the spherical detector, T_p is a function of the source direction and polarization encoded by $\mathbf{f}_s$. Likewise, the lossless limit of T_p, $T_n^{\rm eff}(\mathbf{f}_s)$ and the effective fractional bandwidth $\delta^{\rm eff}(\mathbf{f}_s)$ are also generally dependent on source direction and polarization. Sections IV–VI explore the anisotropy of $T_n^{\rm eff}$ and $\delta^{\rm eff}$ over the sky as a function of the locations and parameters of the transducers attached to the sphere.

IV. SPECIAL TRANSDUCER SYMMETRIES

If the transducer parameters or attachment locations exhibit certain symmetries, then the behavior of $T_n^{\rm eff}(\mathbf{f}_s)$ or $\delta^{\rm eff}(\mathbf{f}_s)$ is simplified considerably. Three symmetries are examined here: (i) identical transducer noise temperatures, (ii) completely identical transducer systems, and (iii) dodecahedral/icosahedral transducer locations. Previous work [16] examined the consequences of each of these symmetries for a spherical detector. The results are summarized below.

As described in Sec. II C, Price [15] showed that $\sigma(\omega)$ for a lossless multimode bar detector equals $e(\omega)/(k_B T_n)$ so that $T_p = T_n$ for any lossless bar detector. For a lossless spherical detector, $e(\omega)$ and $\sigma(\omega)$ are generally no longer proportional to each other, except when all the T_n's of the amplifiers are equal. Then once again $e(\omega)/(k_B T_n) = \sigma(\omega)$ and

$$k_B T_n^{\rm eff}(\mathbf{f}_s) = k_B T_n \quad \text{for all } \mathbf{f}_s . \tag{69}$$

If all the transducer systems not only have equal T_n but are equal in every respect (equal masses, springs, T_n, and Z_n), then this stronger symmetry gives an equivalence with a set of bar detectors: the SNR is the same as if the identical transducer systems were mounted on N separate bar antennas, with effective antenna masses

$$\mu_i = \mu/\eta_i , \quad i = 1, \ldots, N, \tag{70}$$

where the η_i are the eigenvalues of $\mathbf{M}$, and with the signal energy E divided up among the bar antennas in a source-direction- and polarization-dependent way.

This equivalence can be derived as follows. If the transducers are identical, then Eq. (29) shows that a basis which diagonalizes $\mathbf{Y}_{tt}$ also diagonalizes $\mathbf{S}_x$. Furthermore, diag($\mathbf{m}_t s$) and diag($\mathbf{k}_t/s$) are both scalar multiples of the identity matrix, and hence commute with $\mathbf{Y}_0$. Then Eq. (50b) shows that, if an $N\times N$ unitary matrix $\mathbf{U}$ diagonalizes $\mathbf{Y}_0$ (and $\mathbf{M}$), then the $2N\times 2N$ matrix diag($\mathbf{U},\mathbf{U}$) diagonalizes each of the $N\times N$ submatrices in $\mathbf{Y}$, and hence diagonalizes $\mathbf{Y}_{tt}$ in particular. Since the submatrices of $\mathbf{Y}^{-1}$ commute with each other they act as scalars, and $\mathbf{Y}$ may be computed explicitly by applying the formula for the inverse of a 2×2 matrix to the submatrices of $\mathbf{Y}$. If $\mathbf{U}^\dagger \mathbf{M} \mathbf{U} = {\rm diag}(\eta_i)$, then one obtains statistically independent output channels $\mathbf{y} = \mathbf{U}^\dagger \mathbf{x}$. The eigenvalues ζ_i of $\mathbf{S}_x$ [see Eq. (22)] and their contributions to $\sigma(\omega)$ can be read from Eq. (29) using the following eigenvalues of $\mathbf{Y}_{tt}$, $\mathbf{Y}_{ss}$, and $\mathbf{Y}_{ts}$:

$${\rm eig}_i(\mathbf{Y}_{tt}) = \frac{\mu/\eta_i (s + \omega_0^2/s) + m_t s}{(m_t s + k_t/s)\mu/\eta_i (s + \omega_0^2/s) + m_t k_t}, \tag{71}$$

$${\rm eig}_i(\mathbf{Y}_{ss}) = \frac{(m_t s + k_t/s)}{(m_t s + k_t/s)\mu/\eta_i (s + \omega_0^2/s) + m_t k_t}, \tag{72}$$

$${\rm eig}_i(\mathbf{Y}_{ts}) = \frac{-m_t s}{(m_t s + k_t/s)\mu/\eta_i (s + \omega_0^2/s) + m_t k_t}. \tag{73}$$

The above formulas do not explicitly depend on N; their form is always the same as for the case $N=1$. The only difference for $N>1$ is that the effective mass of the antenna μ is replaced by new effective masses μ/η_i. Thus, if the transducers are identical, the total SNR is the sum of SNR's for statistically independent output channels, each of which has a form equivalent to that for a two-mode bar detector, with effective antenna masses for the bars given by the values μ/η_i.

The eigenvalues η_i can readily be found numerically for any given set of transducer locations, but they obey a number of analytical properties. The η_i are non-negative and sum up to N, and at most five of them are nonzero. (The zero eigenvalues are equivalent to infinitely massive bars which do not give transducer signals in response to forces acting on the antenna, but which give useful vetoes against spurious forces acting on a transducer.) As Johnson and Merkowitz discovered [8], if the transducer attachment points are located at the centers of six, nonopposite, faces of a regular dodecahedron, then a very special symmetry exists. From the point of view described here, what is special is that the nonzero η_i's display the maximum, fivefold, degeneracy:

$$\eta_i = N/5, \quad i = 1, \ldots, 5. \tag{74}$$

Fivefold degeneracy is also achieved for ten transducers centered on half the faces of a regular icosahedron. In either case, it does not matter how E is divided up among the equivalent bar detectors since the spectral shape of each contribution to $\sigma(\omega)$ is identical, so Eq. (69) holds true once again, and the total SNR is direction and polarization independent.

As found by Johnson and Merkowitz, the quadrupole components of the antenna motion are statistically independent output channels when the transducers are identical and located with dodecahedral symmetry. This is easily shown using the methods of this paper as follows. Expressing the antenna velocity as $\mathbf{u}_s = \mathbf{G}\mathbf{a}$, where $\mathbf{a}$ is the vector of mode amplitudes, then, in general, $\mathbf{a}$ is found by solving the equation

$$\mathbf{G}\mathbf{a} = \mathbf{Y}_{ss}\mathbf{f}_s \tag{75}$$

$$= \mathbf{Y}_{ss}\mathbf{Y}_{ts}^{-1}\mathbf{x}. \tag{76}$$

If $N>5$, the equations for $\mathbf{a}$ are overdetermined giving $N-5$ veto conditions, but there is always a least-square error solution

$$\mathbf{a} = (\mathbf{G}^{\rm T}\mathbf{G})^{-1}\mathbf{G}^{\rm T}\mathbf{Y}_{ss}\mathbf{Y}_{ts}^{-1}\mathbf{x}. \tag{77}$$

For the dodecahedral (or icosahedral) arrangement, the five quadrupole spherical harmonics are not only orthogonal when integrated over the entire sphere, but also when restricted to the transducer attachment points. Then

$$\mathbf{G}^{\mathrm{T}}\mathbf{G}=\frac{N}{4\pi}\mathrm{diag}(1,1,1,1,1), \tag{78}$$

which according to Eq. (62) implies that the columns of **G** are eigenvectors of **M** each with eigenvalue $\eta=N/5$. Therefore, one can choose the orthogonal matrix **U** so that its first five columns equal $(4\pi/N)^{1/2}\mathbf{G}$. The solution for the mode amplitudes in Eq. (77) then reduces to being proportional to the first five components of $\mathbf{y}=\mathbf{U}^{\dagger}\mathbf{x}$:

$$a_i=\sqrt{\frac{4\pi}{N}}\begin{pmatrix} m_t s+k_t/s \\ -m_t s \end{pmatrix} y_i \tag{79}$$

$$=\sqrt{\frac{4\pi}{N}}\mathrm{eig}_i(\mathbf{Y}_{ss})(\mathbf{U}^{\mathrm{T}}\mathbf{f}_s)_i, \quad \text{for } i=1,\ldots,5. \tag{80}$$

Thus, for a dodecahedral or icosahedral arrangement of transducers, the statistically independent output channels with nonzero coupling to the sphere are proportional to the quadrupole mode amplitudes a_i, and the wave form of each a_i is proportional to the velocity of an effective antenna mass $5\mu/N$ in an equivalent bar detector.

V. EFFECTS OF TRANSDUCER ASYMMETRIES

This section presents the results of numerically evaluating Eqs. (67) and (68) when transducer asymmetries exist. Starting with symmetrically located, identical transducers, various tolerances were relaxed, and T_n^{eff} and δ^{eff} were evaluated on a grid covering the sky using the linear algebra package MATLAB [37].

A. Location asymmetry

Sets of six transducer locations perturbed around regular dodecahedral locations were randomly generated. Using identical, single-mode transducers with parameters chosen to give Price's ''maximally flat'' matching network [15] for effective antenna mass $\mu/\eta=5/6\mu$, one finds asymmetries in δ^{eff} as shown in Figs. 1 and 2 for one trial with 15° tolerance. Price's bandwidth parameter was chosen as $\delta=0.1$, giving a theoretical value $\delta^{\mathrm{eff}}\approx 0.1\pi/2$ for perfect dodecahedral locations. (For single-mode transducers, δ is the square root of the ratio of the transducer mass to the effective antenna mass.) Identical-transducer symmetry implies $T_n^{\mathrm{eff}}=T_n$, but δ^{eff} depends on source direction (ϕ,θ) and polarization state ψ [38].

Single-mode transducer systems were chosen for simplicity, for even though multimode systems may be handled as indicated by Eq. (51), little qualitative difference would be expected in the anisotropy effects. The main effect of using additional resonators is an impedance transformation in which the transducer is made to appear to the antenna as a more massive transducer with a larger noise impedance [15]. To achieve the order 15% fractional bandwidths assumed in the examples presented here, existing or projected transducer technology would likely require at least two-mode transducer systems [11], but this will not affect the conclusions derived here.

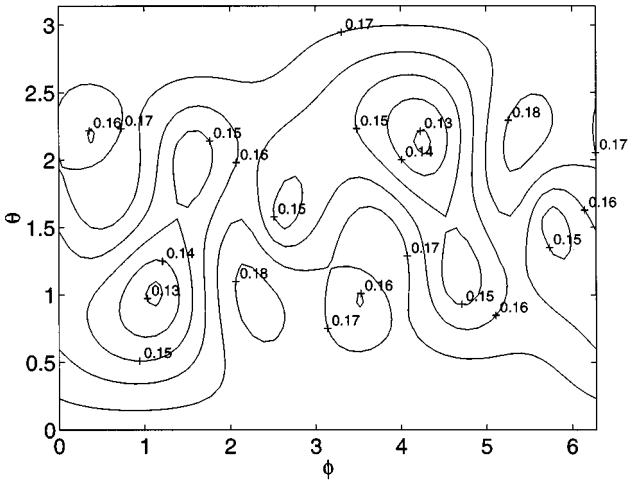

FIG. 1. Bandwidth anisotropy for a dodecahedral arrangement with 15° location tolerance. Plot of $\max_{\psi}(\delta^{\mathrm{eff}})$ versus (ϕ,θ); $\max_{\theta,\phi,\psi}(\delta^{\mathrm{eff}})=0.184$.

Figure 3 helps explain how the bandwidth asymmetry develops by showing the eigenvalues κ of $\mathbf{K}_0(\omega)$. The analysis of identical-transducer symmetry in Sec. IV shows that the shapes of the five nonzero κ_i's are the shapes of $\sigma(\omega)$ for the equivalent bar detectors. Some of the η_i's are larger (smaller) than the 6/5 for the symmetrical case, corresponding to a lighter (heavier) bar, increasing (decreasing) the mode splitting and bandwidth. Depending on (ϕ,θ,ψ), the channels are weighted differently in $\sigma(\omega)$ giving rise to the δ^{eff} asymmetry.

Figure 4 summarizes the results of all the random trials and shows that, as expected, deviation from regular dodecahedral locations increases δ^{eff} for some directions and polarizations, and decreases it for others. From the figure, it is also apparent that the size of the asymmetry grows linearly in the angular tolerance.

B. Tuning asymmetry

Figure 5 shows a maximally flat transducer system with perfect locations but mistuned spring constants deviating up

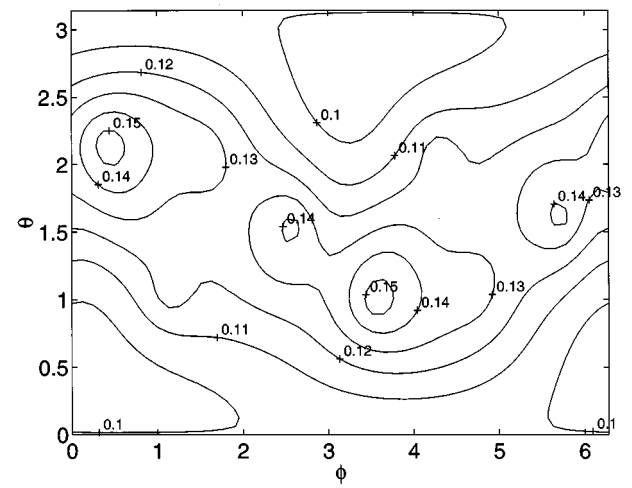

FIG. 2. Plot of $\min_{\psi}(\delta^{\mathrm{eff}})$ versus (ϕ,θ) for the example in Fig. 1; $\min_{\theta,\phi,\psi}(\delta^{\mathrm{eff}})=0.095$.

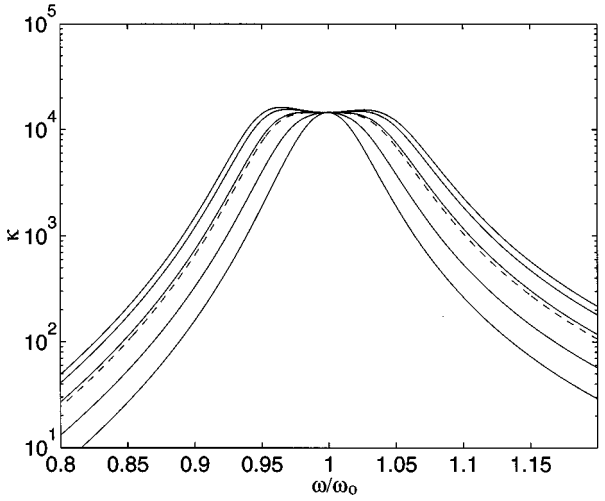

FIG. 3. Eigenvalues κ of SNR kernal $\mathbf{K}_0(\omega)$ for the example in Fig. 1; η={1.67,1.53,1.26,0.89,0.64} giving bandwidths of {0.18,0.17,0.15,0.12,0.09}. Dashed line: fivefold κ for perfect symmetry has $\delta^{\text{eff}}=0.15$.

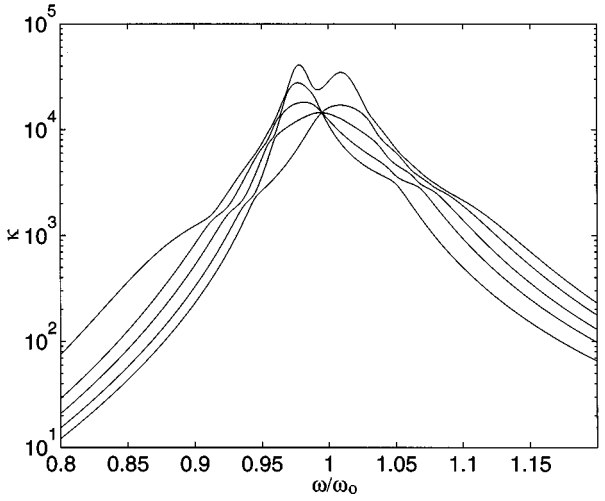

FIG. 5. Eigenvalues κ of the SNR kernal $\mathbf{K}_0(\omega)$ for a regular dodecahedral arrangement with 20% tolerance on transducer spring constants. This example has spring constants perturbed by factors 1.072, 1.174, 0.953, 1.008, 1.132, 0.814.

to 20%. The transducers are thus not identical and equivalence to a set of bar detectors is lost; however, T_n symmetry still gives $T_n^{\text{eff}} = T_n$, so one only need look at δ^{eff} asymmetry. Figure 6 shows that δ^{eff} is always decreased, substantially for some directions and polarizations, but hardly at all for others. The effect is second order in spring constant tolerance.

C. Noise temperature asymmetry

The final asymmetry considered here is variable T_n but identical Z_n. Figure 7 shows an example for 20% T_n tolerance. Since both the identical-transducer and identical-T_n symmetries are broken, one might expect both δ^{eff} and T_n^{eff} to be anisotropic, however, the numerical results show that, although the κ become nondegenerate, they all retain the same shape as for the symmetric case. Thus δ^{eff} is unchanged. Figure 8 summarizes the results and shows that T_n^{eff} asymmetry develops linearly with the tolerance, and respects the bounds from Eq. (41):

$$\min(T_n) \leqslant T_n^{\text{eff}}(\mathbf{f}_s) \leqslant \max(T_n). \tag{81}$$

In fact, the numerical results show that there are usually directions and polarizations for which T_n^{eff} is quite close to $\max(T_n)$ or $\min(T_n)$.

VI. ALTERNATIVE TRANSDUCER LOCATIONS

Calculation of SNR anisotropy can be used to evaluate the merits of alternative transducer locations relative to the

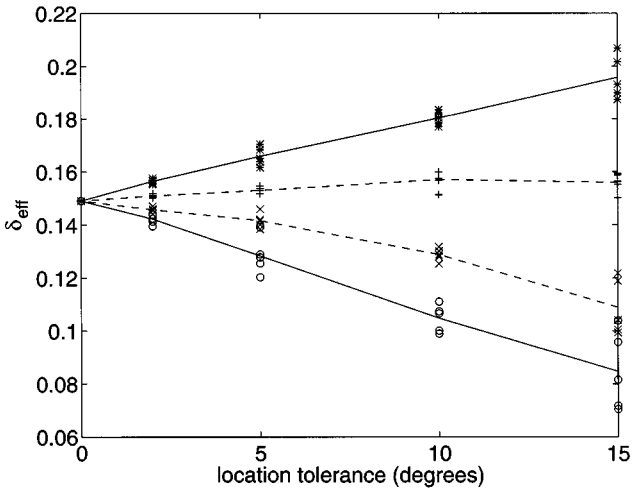

FIG. 4. Fractional bandwidth for dodecahedral arrangements with 0°–15° location tolerance. Plotted for each random trial are: max (∗) and min (○) of δ^{eff}, and max (+) and min (×) of $\langle \delta^{\text{eff}} \rangle_\psi$. Lines join averages of trials at each tolerance.

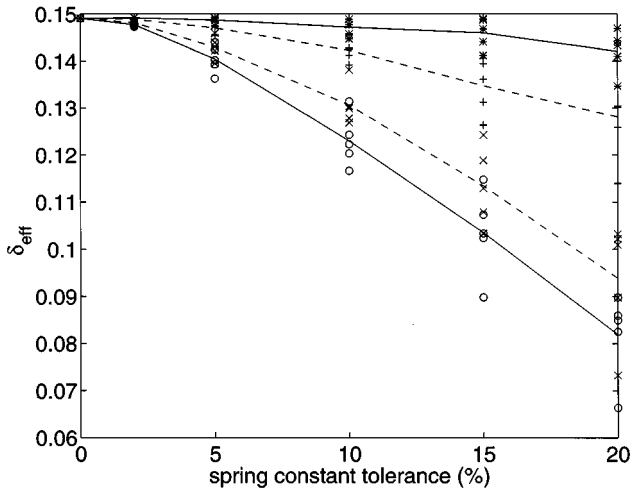

FIG. 6. Maximum and minimum effective bandwidth for regular dodecahedral arrangements with 0–20 % spring tolerance. Plotted for each random trial are the max (∗) and min (○) of δ^{eff} and max (+) and min (×) of $\langle \delta^{\text{eff}} \rangle_\psi$. Lines join averages of trials at each tolerance.

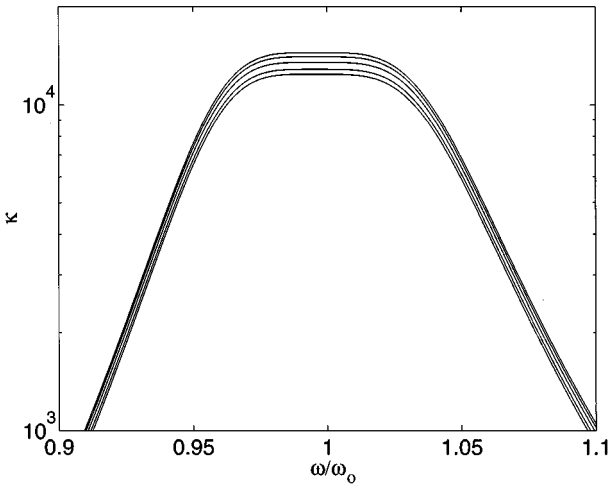

FIG. 7. Eigenvalues κ of the SNR kernal $\mathbf{K}_0(\omega)$ for a regular dodecahedral arrangement with 20% tolerance on T_n. For this example, T_n=0.999,1.182,1.099,1.022,1.156,1.050.

dodecahedral arrangement. The regular dodecahedral and icosahedral arrangements with identical transducers are special in that they give isotropic and polarization-independent SNR. So far this paper has examined the effects of perturbations around the regular dodecahedral arrangement with identical transducers. One might also ask what happens if large changes are made in transducer locations or parameters. For example, how anisotropic is the SNR for other transducer arrangements which have been proposed [20], and how robust is the regular dodecahedral arrangement under a failure of one transducer?

A. Five or six transducers?

Lobo and Serrano have proposed using only five transducers, instead of six, to monitor the five spheroidal quadrupole modes [20]. Rather than seeking to maximize the degeneracy in the eigenvalues η which determine the coupled mode frequencies, they suggested placing five transducers equally spaced around the sphere's north pole at a latitude chosen to give approximately equally spaced mode splittings. They felt that this criterion might yield a preferred location for the transducers, and they found that the resulting angle between the pole and the transducers θ=1.180 allowed the transducers to be placed on five of the 60 faces of a pentagonal hexacontahedron. Another reasonable sounding criterion for placing five transducers might be to choose their latitude so that the ratio between the largest and smallest mode splittings is made as small as possible to try to approximate the dodecahedral behavior.

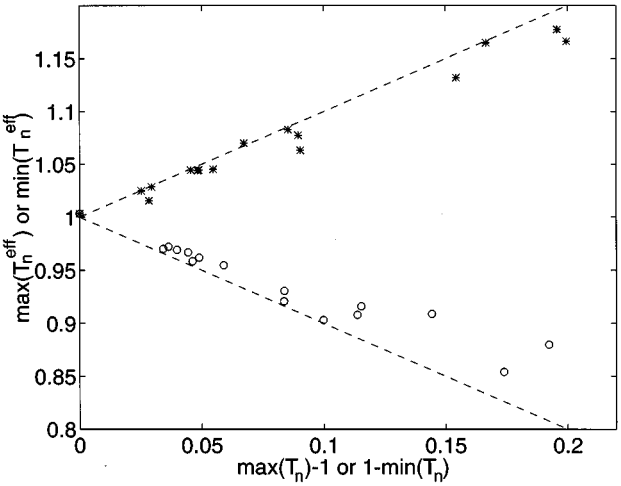

FIG. 8. Maximum and minimum effective noise temperature for a regular dodecahedral arrangement with 0, 5, 10, and 20 % T_n tolerances. Values of max(T_n^{eff}) and min(T_n^{eff}) are plotted versus max(T_n)−1 or 1−min(T_n), respectively.

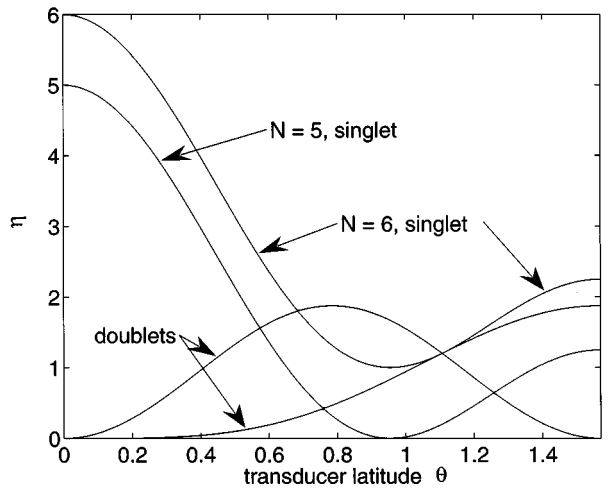

FIG. 9. Nonzero eigenvalues η (which determine equivalent bar antenna masses) versus transducer latitude θ for fivefold arrangements of transducers with or without a transducer at the north pole. In both cases, the five eigenvalues form a singlet and two doublets. The curves for the doublets are the same with or without a polar transducer.

The Lobo-Serrano arrangement and the minimal-splitting-ratio criterion can be rigorously evaluated in terms of the anisotropy they produce in δ^{eff}. Figure 9 shows the eigenvalues η as functions of the latitude θ at which five transducers are placed, equally spaced in longitude, with or without a sixth transducer at the pole. The nonzero eigenvalues form a singlet and two doublets. For θ=0.9553, N=5 gives only four nonzero eigenvalues because all transducers lie on nodes of ψ_0. The dodecahedral arrangement of six transducers occurs at θ=1.1071 and gives the maximal fivefold degeneracy with all η=6/5, as shown in Eq. (74). The Lobo-Serrano pentagonal hexacontahedral arrangement is θ=1.180, N=5. The minimal splitting ratio criterion for five transducers is achieved at θ=1.258, where there is a degeneracy between the singlet and one doublet, giving a maximal value of 0.416 for min(η_i)/max(η_i).

Figure 10 compares δ^{eff} for the three proposed transducer arrangements. The pentagonal hexacontahedral arrangement is highly anisotropic and polarization dependent with δ^{eff} varying by about a factor of 2 over the sky and, although it gives greater bandwidth for sources over the poles, for some polarizations it gives inferior bandwidth (and hence inferior sensitivity if antenna dissipation is not negligible) than the dodecahedral arrangement over 78% of the area on the sky. The minimal-splitting-ratio arrangement is less polarization

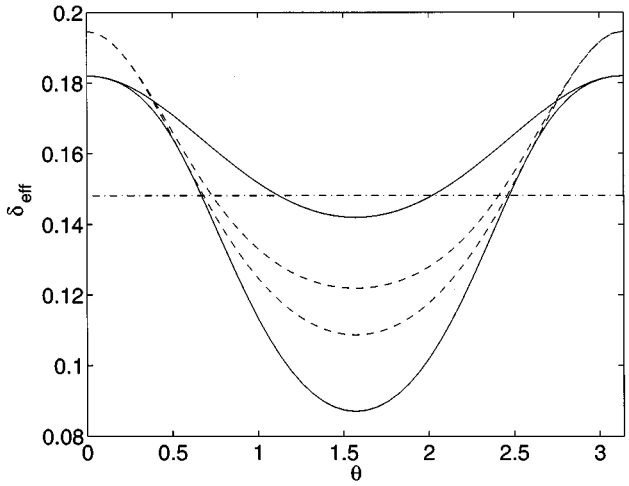

FIG. 10. Effective bandwidth $\delta_{\rm eff}$ versus source direction θ for three cases: the Lobo-Serrano arrangement (solid curves), the $\theta=1.258, N=5$ arrangement (dashed curves), and the regular dodecahedral arrangement (dash-dot line). For each case, maximum and minimum bandwidth over all polarization states are shown.

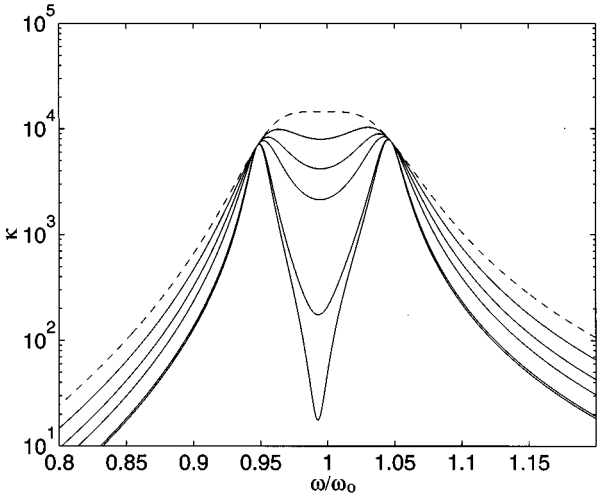

FIG. 11. Eigenvalues of $\mathbf{K}_0(\omega)$ for a regular dodecahedral arrangement with excess additive noise in one transducer. Four of five nonzero eigenvalues remain unchanged (dashed curve). The fifth decreases as S_u increases ($S_u=2,4,8,100,1000$) for the bad transducer. The $S_u=1000$ curve essentially gives the limit $S_u\to\infty$.

dependent than the pentagonal hexacontahedral arrangement and gives even larger bandwidth at the poles, but it is also inferior to the dodecahedral arrangement over most of the sky.

B. Excess additive noise in one transducer

If six or ten transducers need to be placed on a spherical antenna to give an optimal, isotropic sensitivity, how robust is the detector to a failure of one transducer? There are several ways in which a transducer could fail. This section examines the effects of excess additive noise in one transducer. For both the dodecahedral and icosahedral maximally flat systems, $T_n^{\rm eff}$ and $\delta^{\rm eff}$ were calculated as S_u for one of the transducers was gradually increased to infinity. The limit of infinite S_u corresponds to a transducer which gives no signal output. The value of S_f for the bad transducer is assumed to be the same as for the other transducers.

Figure 11 shows the effects of excess additive noise on the SNR eigenvalues κ using the dodecahedral arrangement. Four of the eigenvalues remain unchanged, but one develops a zero near $\omega=\omega_0$.

Figures 12 and 13 show that $T_n^{\rm eff}$ and $\delta^{\rm eff}$ are unaffected by the excess noise for a source directly over the bad transducer. This is to be expected since such a source excites a sphere mode which has no coupling to that transducer. One finds that $T_n^{\rm eff}$ and $\delta^{\rm eff}$ depend only on the spherical angle $\Delta\theta$ between the bad transducer and the source direction. On a band around the sky 90° from the bad transducer, $\max_\psi(T_n^{\rm eff})$ is degraded by a factor of 2.4. The corresponding value of $\delta^{\rm eff}$ is degraded by a factor of 1.9, further eroding the sensitivity if antenna dissipation is significant.

If the regular icosahedral arrangement is used instead, figures analogous to Figs. 11–13 look very similar, except for their vertical scale. Once again, a zero develops in one of the κ values, $T_n^{\rm eff}$ and $\delta^{\rm eff}$ are unaffected for a source directly over the bad transducer, and they depend only on the source-transducer angle $\Delta\theta$.

The relative robustness of the dodecahedral and icosahedral arrangements is compared in Figs. 14–16 with $S_u=1000$ for the bad transducer, which practically gives the limiting behavior for $S_u\to\infty$. The worst case value of $T_n^{\rm eff}$ is better by a factor of 1.6 for the icosahedral arrangement, and the corresponding $\delta^{\rm eff}$ is better by a factor of 1.8. It should be pointed out, however, that the mass for the icosahedral transducers was chosen to be 6/10 times that for the dodecahedral transducers so as to scale with the lighter effective antenna mass in the icosahedral case. However, if the transducer design has S_f dominated by amplifier back-action noise rather than by transducer mechanical dissipation, then it is more reasonable to assume that Z_n is held fixed rather than the mass ratio $m/(\mu/\eta)$. Then the single-mode, icosahedral transducers would optimally be lighter by $(6/10)^{1/3}=0.84$

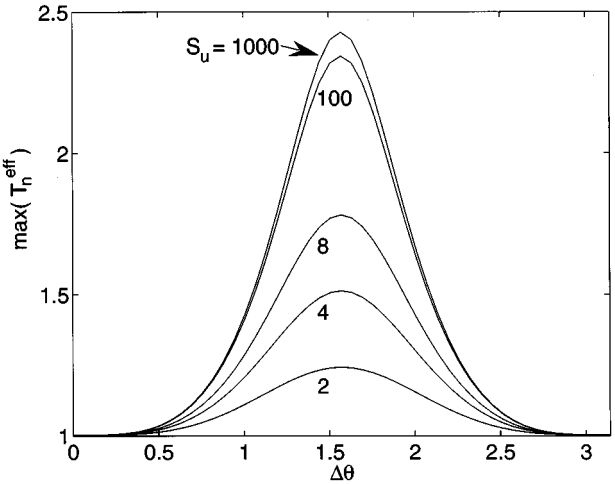

FIG. 12. Effective noise temperature for a regular dodecahedral arrangement with excessive additive noise in one transducer. Worst case $T_n^{\rm eff}$ (maximum over source polarization) plotted versus the angle $\Delta\theta$ between the bad transducer and the source direction.

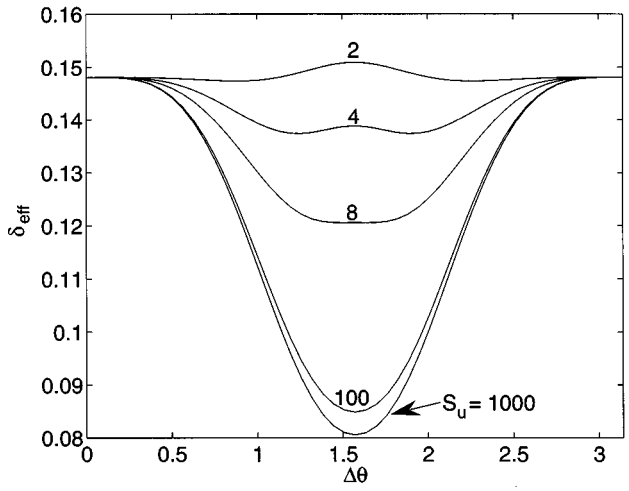

FIG. 13. Effective bandwidth for a regular dodecahedral arrangement with excess additive noise in one transducer. Value of δ_{eff} giving $\max(T_n^{\text{eff}})$ is plotted versus $\Delta\theta$.

giving an increase in bandwidth by a factor of $(10/6)^{1/3} = 1.19$ when all transducers are good. Therefore, when one transducer is very bad, one would expect δ^{eff} to be larger for the icosahedral arrangement by 1.19 for sources over the bad transducer and $1.8 \times 1.19 = 2.1$ for sources 90° away.

Thus the icosahedral arrangement is modestly more robust against a transducer failure, with improvements in worst case T_n^{eff} and δ^{eff} by roughly the ratio of the numbers of transducers used, but whether this effect is enough to justify using $N=10$ transducers instead of $N=6$ will depend on the cost of an increased number of transducers in terms of system complexity and increased risk of failure weighed against the benefits of lighter transducer masses or enhanced bandwidth.

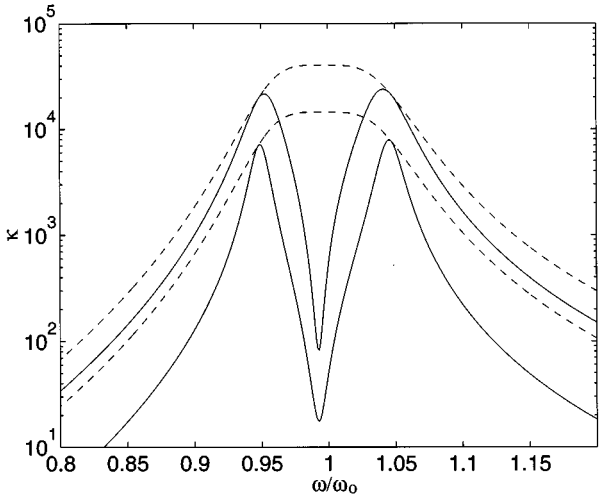

FIG. 14. Eigenvalues of $\mathbf{K}_0(\omega)$ for regular dodecahedral (lower dashed and solid curves) and icosahedral (upper dashed and solid curves) arrangements when one transducer has excess additive noise. Four of the nonzero eigenvalues are unaffected by the excess noise (dashed curves). The fifth decreases to a limiting value (solid curves) as $S_u \to \infty$.

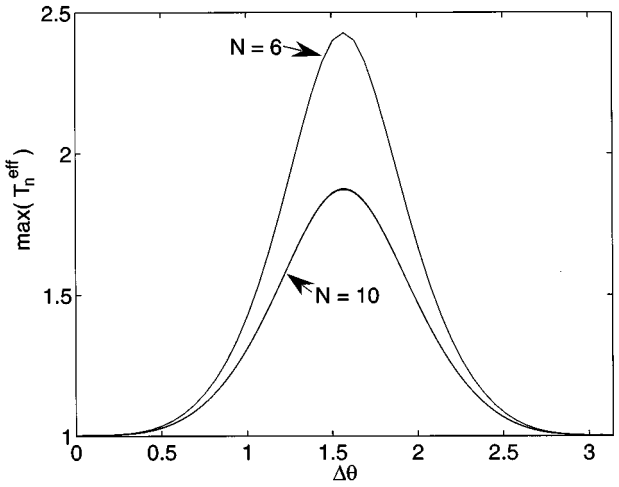

FIG. 15. Effective noise temperature for regular dodecahedral ($N=6$) and icosahedral ($N=10$) arrangements when one transducer has $S_u \to \infty$. Worst case T_n^{eff} (maximum over source polarization) is plotted versus the angle $\Delta\theta$ between the bad transducer and the source direction.

VII. MAXIMUM LIKELIHOOD ESTIMATION

The theory developed in Secs. II and III can be applied to investigate other questions. For example, how accurately can signal parameters such as the source direction and polarization be reconstructed? Magalhães *et al.* [39] gave a method of solving for the signal and polarization when noiseless, radial, nonresonant transducers are used to monitor a spherical antenna. Zhou and Michelson [9] used analytical and Monte Carlo methods to find the accuracy of estimated parameters in the case where linear combinations of resonant transducer outputs which give the amplitudes of the antenna's quadrupole modes are five statistically independent channels all with identical noise. This happens for the Zhou-Michelson independent transducer arrangement and, as explained in Sec. IV, also for the dodecahedral and icosahedral arrangements of identical transducers. Merkowitz and

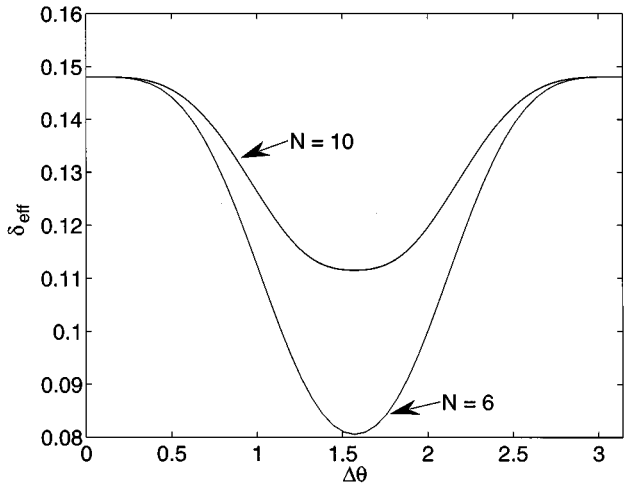

FIG. 16. Bandwidth for regular dodecahedral ($N=6$) and icosahedral ($N=10$) arrangements when one transducer has $S_u \to \infty$. The value of δ^{eff} giving $\max(T_n^{\text{eff}})$ is plotted versus the angle $\Delta\theta$.

Johnson [19] have also investigated the reconstruction problem experimentally with a prototype truncated icosahedral gravitational wave antenna (TIGA). To investigate estimation accuracy for an asymmetrical detector analytically, the explicit formula for $\sigma(\omega)$ given by Eq. (63) can be used together with the connection between optimal filtering and the likelihood ratio described in Sec. II A.

Just as for the signal detection problem, there exists a well developed theory for the signal estimation problem [23], but the literature appears to be lacking formulas written in a form so that they may be easily applied to a detector with vector output in general, and to a spherical gravitational wave detector in particular. This section first briefly develops the required formulas, and then applies them to determine the accuracy of signal reconstruction for a spherical detector.

A. Estimation theory for a detector with vector output

The first formula needed is one which shows explicitly how to calculate the likelihood ratio λ comparing the probabilities of observing the data under the hypotheses H_0, the data $\mathbf{x}$ is only noise, and H_1, the data is noise plus a known signal $\mathbf{x}_{\rm sig}(\boldsymbol{\alpha})$, where $\boldsymbol{\alpha}$ is a vector listing the various signal parameters on which $\mathbf{x}_{\rm sig}$ depends. The explicit formula for λ can be derived somewhat laboriously by assuming that the components of $\mathbf{x}$ are sampled at a large number of discrete times, and then writing down and manipulating a generalized version of Eq. (4) which takes into account the correlations between all the samples. However, the same result can be obtained much more quickly by starting with the abstract result for $\ln\lambda$ given by Eq. (5), and using the abstract formula for the peak output of the optimal linear filter Eqs. (7) and (9) to substitute in the explicit form found for the optimal linear filter for a detector with vector output Eqs. (11), (14), and (16). The result is

$$\ln\lambda = (\mathbf{x}_{\rm sig},\mathbf{x})_x - \frac{1}{2}(\mathbf{x}_{\rm sig},\mathbf{x}_{\rm sig})_x , \tag{82}$$

where $(\ ,\ )_x$ is a convenient notation for the inner product defined by

$$(\mathbf{a},\mathbf{b})_x = \int_{-\infty}^{\infty} \mathbf{a}^{\dagger}(\omega)\mathbf{S}_x^{-1}(\omega)\mathbf{b}(\omega)\frac{d\omega}{2\pi}. \tag{83}$$

[This is a real-valued inner product if $\mathbf{a}(t)$ and $\mathbf{b}(t)$ are real.] In words, Eq. (82) says that $\ln\lambda$ equals the (peak) output of the optimal linear filter designed for $\mathbf{x}_{\rm sig}$ when applied to the data $\mathbf{x}$, minus one-half the filter output when applied to $\mathbf{x}_{\rm sig}$, this latter quantity also being the variance of the noisy filter output according to Eq. (15).

The usefulness of a concrete formula for λ stems from the connection between λ and estimation of signal parameters. Just as for the detection problem for a known signal, one reasonable criterion for forming estimates of unknown parameters is to assign costs for errors in the estimates, and then to choose the estimates so as to minimize the expected cost (the Bayes criterion). If the cost function is the mean-square error, then the optimal estimate is to compute the mean of the *a posteriori* probability distribution

$$P(\boldsymbol{\alpha}|\mathbf{x}) = \frac{P(\mathbf{x}|\boldsymbol{\alpha})P(\boldsymbol{\alpha})}{P(\mathbf{x})}. \tag{84}$$

If a cost function is not given, then a reasonable criterion is to choose the most likely value of $\boldsymbol{\alpha}$ given the data, i.e., choose the mode rather than the mean of the *a posteriori* distribution. If the *a priori* probabilities $P(\boldsymbol{\alpha})$ are unknown or nearly uniform, then maximizing $P(\boldsymbol{\alpha}|\mathbf{x})$ is equivalent to maximizing $P(\mathbf{x}|\boldsymbol{\alpha})$ or to maximizing the conditional likelihood ratio

$$\lambda = \frac{P(\mathbf{x}|\boldsymbol{\alpha})}{P_0(\mathbf{x})}. \tag{85}$$

Finding the value for $\boldsymbol{\alpha}$ which maximizes λ produces the *maximum likelihood estimate* $\hat{\boldsymbol{\alpha}}$.

Two desirable properties of an estimator are that it be *unbiased* (the mean of estimated values should equal the true parameter values) and *efficient* (have the lowest possible variance given by the Cramer-Rao bound described below). If an unbiased efficient estimator exists, then it can be shown to equal the maximum likelihood estimator (see Sec. 10.5 of [23]), and it is often found that the maximum likelihood estimator approaches the minimum variance bound as the SNR gets large. The Cramer-Rao bound [40] gives a formula for the covariance matrix of an unbiased efficient estimator which can be evaluated using λ. If there are several unknown parameters, then the Cramer-Rao bound involves ''Fisher's information matrix'' $\boldsymbol{\gamma}$, which has elements

$$\gamma_{ij} = E\left[\frac{\partial \ln P(\mathbf{x}|\boldsymbol{\alpha})}{\partial\alpha_i}\,\frac{\partial \ln P(\mathbf{x}|\boldsymbol{\alpha})}{\partial\alpha_j}\right] \tag{86a}$$

$$= E\left[\frac{\partial \ln\lambda(\boldsymbol{\alpha})}{\partial\alpha_i}\,\frac{\partial \ln\lambda(\boldsymbol{\alpha})}{\partial\alpha_j}\right], \tag{86b}$$

where the expectation value in the above equations is the conditional expectation given the value of $\boldsymbol{\alpha}$ and the derivatives are supposed to be evaluated at the true value of $\boldsymbol{\alpha}$. Then the covariance matrix of the unbiased efficient estimator is the inverse of Fisher's matrix,

$$\sigma^2_{\hat{\alpha}_i\hat{\alpha}_j} = (\boldsymbol{\gamma}^{-1})_{ij}. \tag{87}$$

Equation (87) gives a powerful way to evaluate the accuracy of maximum likelihood estimates once it is seen how to evaluate the expectation values which appear. From Eq. (82), when evaluated at the true parameter values, the derivatives of the log-likelihood ratio are

$$\frac{\partial \ln\lambda(\boldsymbol{\alpha})}{\partial\alpha_i} = \left(\frac{\partial\mathbf{x}_{\rm sig}}{\partial\alpha_i},\mathbf{x}\right)_x - \left(\frac{\partial\mathbf{x}_{\rm sig}}{\partial\alpha_i},\mathbf{x}_{\rm sig}\right)_x \tag{88a}$$

$$= \left(\frac{\partial\mathbf{x}_{\rm sig}}{\partial\alpha_i},\mathbf{n}\right)_x \tag{88b}$$

$$= \int_{-\infty}^{\infty}\frac{d\omega}{2\pi}\left(\frac{\partial\mathbf{x}_{\rm sig}}{\partial\alpha_i}\right)^{\dagger}\mathbf{S}_x^{-1}\mathbf{n}(\omega), \tag{88c}$$

where $\mathbf{n}=\mathbf{x}-\mathbf{x}_{\rm sig}$ is the noise in the data. Thus the Fisher matrix elements are

$$\gamma_{ij}=\int_{-\infty}^{\infty}\frac{d\omega}{2\pi}\int_{-\infty}^{\infty}\frac{d\omega'}{2\pi}\left(\frac{\partial\mathbf{x}_{\rm sig}(\omega)}{\partial\alpha_i}\right)^{\dagger}\mathbf{S}_x^{-1}(\omega)$$

$$\times E[\mathbf{n}(\omega)\mathbf{n}^{\dagger}(\omega')]\mathbf{S}_x^{-1}(\omega')\frac{\partial\mathbf{x}_{\rm sig}(\omega')}{\partial\alpha_j} \tag{89a}$$

$$=\int_{-\infty}^{\infty}\frac{d\omega}{2\pi}\int_{-\infty}^{\infty}\frac{d\omega'}{2\pi}\left(\frac{\partial\mathbf{x}_{\rm sig}(\omega)}{\partial\alpha_i}\right)^{\dagger}\mathbf{S}_x^{-1}(\omega)2\pi\delta(\omega-\omega')$$

$$\times\mathbf{S}_x(\omega)\mathbf{S}_x^{-1}(\omega')\frac{\partial\mathbf{x}_{\rm sig}(\omega')}{\partial\alpha_j} \tag{89b}$$

$$=\left(\frac{\partial\mathbf{x}_{\rm sig}}{\partial\alpha_i},\frac{\partial\mathbf{x}_{\rm sig}}{\partial\alpha_j}\right)_x, \tag{89c}$$

where in the second line the Wiener-Khintchine theorem [41] was used to express $\mathrm{E}[\mathbf{nn}^{\dagger}]$ in terms of $\mathbf{S}_x$. The matrix elements can be expressed even more neatly by defining

$$\chi(\boldsymbol{\alpha},\boldsymbol{\alpha}')=(\mathbf{x}_{\rm sig}(\boldsymbol{\alpha}),\mathbf{x}_{\rm sig}(\boldsymbol{\alpha}'))_x, \tag{90}$$

for then

$$\gamma_{ij}=\left.\frac{\partial^2\chi}{\partial\alpha_i\partial\alpha_j'}\right|_{\boldsymbol{\alpha}=\boldsymbol{\alpha}'}. \tag{91}$$

Equation (91) is used below to study the uncertainties in signal estimation for a spherical gravitational wave detector by explicitly evaluating χ and its derivatives. The function χ is what would be called the ''ambiguity function'' in radar detection theory [42]. The physical significance of χ can perhaps be made clearer by noting that $\chi(\boldsymbol{\alpha},\boldsymbol{\alpha}')$ is the peak output of an optimal filter designed to detect $\mathbf{x}_{\rm sig}(\boldsymbol{\alpha})$ when the actual data is $\mathbf{x}_{\rm sig}(\boldsymbol{\alpha}')$, and $\chi(\boldsymbol{\alpha},\boldsymbol{\alpha})$ is the variance of that filter's noisy output, so that the SNR obtained when using the wrong optimal filter to detect $\mathbf{x}_{\rm sig}(\boldsymbol{\alpha}')$ is

$$S/N=\frac{[\chi(\boldsymbol{\alpha},\boldsymbol{\alpha}')]^2}{\chi(\boldsymbol{\alpha},\boldsymbol{\alpha})}. \tag{92}$$

The more sharply peaked χ is about $\boldsymbol{\alpha}=\boldsymbol{\alpha}'$, the more accurately the true value of $\boldsymbol{\alpha}$ can be estimated.

B. Ambiguity function for a spherical GW detector

The ambiguity function χ for a spherical gravitational wave detector can be evaluated using the results of Sec. III. The expected signal is $\mathbf{x}_{\rm sig}(\omega)=\mathbf{Y}_{ts}\mathbf{f}_s$ with $\mathbf{f}_s$ given in terms of the source direction (θ,ϕ) and $h_+(\omega)$ and $h_\times(\omega)$ according to Eqs. (59) and (60). If the signal power spectrum is essentially flat over the detector's bandwidth, then $h_+(\omega)$ and $h_\times(\omega)$ can be parametrized as

$$h_+(\omega)=h\cos\beta e^{j\,\mathrm{sgn}(\omega)\epsilon_+-j\omega\tau}, \tag{93a}$$

$$h_\times(\omega)=h\sin\beta e^{j\,\mathrm{sgn}(\omega)\epsilon_\times-j\omega\tau}, \tag{93b}$$

where h, β, ϵ_+, $\epsilon_\times$, and τ are real parameters describing respectively the total magnitude of the strain spectrum, the relative magnitudes of the polarization amplitudes, the phases of the two amplitudes, and the signal's arrival time. Thus $\boldsymbol{\alpha}$ consists of these five parameters and (θ,ϕ). The ambiguity function is then

$$\chi(\boldsymbol{\alpha},\boldsymbol{\alpha}')=\int_{-\infty}^{\infty}\frac{d\omega}{2\pi}\mathbf{f}_s^{\dagger}(\omega;\boldsymbol{\alpha})\mathbf{K}(\omega)\mathbf{f}_s(\omega;\boldsymbol{\alpha}') \tag{94a}$$

$$=2\,\mathrm{Re}\left[\int_0^{\infty}\frac{d\omega}{2\pi}\mathbf{f}_s^{\dagger}(\omega;\boldsymbol{\alpha})\mathbf{K}(\omega)\mathbf{f}_s(\omega;\boldsymbol{\alpha}')\right] \tag{94b}$$

$$=2\,\mathrm{Re}\left[\mathbf{f}_s^{\dagger}(\omega_0;\boldsymbol{\alpha}|_{\tau=0})\int_0^{\infty}\frac{d\omega}{2\pi}e^{-j\omega(\tau'-\tau)}\mathbf{K}(\omega)\right.$$

$$\left.\times\mathbf{f}_s(\omega_0;\boldsymbol{\alpha}'|_{\tau'=0})\right]. \tag{94c}$$

C. Lossless narrow-band spherical detector with identical T_n's

Consider first the case of a spherical detector which is lossless, narrow band, and has identical T_n symmetry. (Other cases are considered below, but this case provides a connection with the Zhou-Michelson work [9].) With these assumptions, Eq. (94c) for χ simplifies considerably. If the bandwidth of the detector is so narrow that it is not useful to model the signal phase and arrival time independently (see Sec. VIIE), or if the arrival time τ is known exactly by other means, then τ can be set to zero and removed as a signal parameter. If the detector is lossless, so that thermal noise is absent, then $\mathbf{K}=\mathbf{K}_0$. For a lossless detector with identical T_n symmetry, $k_BT_n^{\rm eff}=k_BT_n$ for all signals $\mathbf{f}_s$, so from Eq. (67) the integral of $\mathbf{K}_0$ must be

$$\int_{-\infty}^{\infty}\frac{d\omega}{2\pi}\mathbf{K}_0(\omega)=\frac{1}{2\mu k_BT_n}\mathbf{M}, \tag{95}$$

independent of the transducer locations and other parameters. Substituting this result into Eq. (94c) with $\tau=0$, and using Eqs. (60) and (62), the formula for χ simplifies to

$$\chi(\boldsymbol{\alpha},\boldsymbol{\alpha}')=\frac{1}{2\mu k_BT_n}\mathrm{Re}[\mathbf{f}_s^{\dagger}(\omega_0;\boldsymbol{\alpha})\mathbf{M}\mathbf{f}_s(\omega_0;\boldsymbol{\alpha}')] \tag{96a}$$

$$=\frac{1}{2k_BT_n}\mathrm{Re}[\mathbf{f}_m^{\dagger}(\omega_0;\boldsymbol{\alpha})\mathbf{f}_m(\omega_0;\boldsymbol{\alpha}')]. \tag{96b}$$

Before proceeding to evaluate the Fisher matrix and its inverse, the estimation covariance matrix, it is worth commenting that the expression for χ given by Eq. (96b) is *precisely the same ambiguity function* which would apply if the Zhou-Michelson independent arrangement of five transducers was used instead of the arbitrarily located, statistically dependent, nonidentical (radial) transducer channels for which Eq. (96b) was derived here. This is easily seen: since the Zhou-Michelson proposed transducers are designed to independently monitor the five quadrupole mode amplitudes of the antenna with the same noise in each channel, an optimal filter designed for an impulsive force with signal parameters $\boldsymbol{\alpha}$ but acting on a signal with parameters $\boldsymbol{\alpha}'$ gives an

output proportional to the sum of the expected mode amplitudes times the actual mode amplitudes [see Eqs. (7) and (9)], but this is exactly what Eq. (96b) prescribes. Therefore, for a lossless spherical narrow-band detector with identical T_n symmetry, not only is the SNR for detecting a known signal independent of the other transducer parameters, but *so is the detector's ambiguity function, and hence also its direction and polarization reconstruction accuracy.* This result shows rigorously that the results of the Zhou-Michelson analysis apply to a much broader class of detectors.

In fact, the assumptions of a spherical antenna and radial transducers are *not* needed for Eq. (96b) to hold. All that is needed is for the detector to be lossless, the noise temperatures to be identical, and the signal to be impulsive. Then $\mathbf{K}_0(\omega)$ will still integrate to a constant matrix $\mathbf{M}$, which, even though its elements are no longer given by Eq. (48), must give for $\chi(\boldsymbol{\alpha},\boldsymbol{\alpha}')$, a bilinear form in $\mathbf{f}_m(\omega_0;\boldsymbol{\alpha})$ and $\mathbf{f}_m(\omega_0;\boldsymbol{\alpha}')$ which evaluates to $E/(k_B T_n)$ for $\boldsymbol{\alpha}=\boldsymbol{\alpha}'$. Since the energy E deposited by the impulsive signal in an antenna initially at rest is a quantity dependent only on the antenna and not the transducers and since Eq. (56) is a general expression for E requiring only knowledge of the eigenmodes of the bare antenna without transducers, Eq. (96b) is seen to hold in general. The *ambiguity function*, and hence also *the signal reconstruction accuracy*, of a lossless narrow-band detector with identical T_n symmetry is independent of the other transducer parameters. Of course, if the antenna is not spherical, then $\mathbf{f}_m$ will not be given by Eq. (59) and E will generally depend on source direction and polarization. Similarly, if the antenna is spherical but there are less than $N=5$ distinct transducer locations, then the transducers will not couple to all the degenerate quadrupole modes and some of the energy in the quadrupole modes will be hidden from the transducers and should not be included in E, which will then be direction and polarization dependent.

Next, it is shown that evaluating the estimation covariance matrix by the abstract techniques described above does indeed reproduce the Zhou-Michelson results obtained by more direct analytical and Monte Carlo methods (plus giving some analytical formulas they missed), with the difference that the results are valid now for *any* lossless, narrow-band, spherical detector with $N\geqslant 5$ radial or nonradial transducers having identical T_n's. This serves to illustrate the abstract techniques before they are applied to analyze the effects of breaking the T_n symmetry, for example.

Substituting Eq. (59) for $\mathbf{f}_m$ and Eqs. (93a) and (93b) for h_+ and $h_\times$ into Eq. (96b) gives an explicit analytical formula for χ from which its derivatives and the Fisher matrix elements γ_{ij} can be computed from Eq. (91). The calculations are straightforward, but tedious by hand. The program MATHEMATICA [43] is helpful in finding the nonzero elements of the symmetric matrix $\boldsymbol{\gamma}$,

$$\gamma_{hh}=h^{-2}S/N, \tag{97a}$$

$$\gamma_{\theta\theta}=S/N, \tag{97b}$$

$$\gamma_{\phi\phi}=(1+3\cos^2\theta)S/N, \tag{97c}$$

$$\gamma_{\phi\beta}=-2\cos\Delta\epsilon\ \cos\theta\ S/N, \tag{97d}$$

$$\gamma_{\phi\epsilon_+}=\sin\Delta\epsilon\ \cos\theta\ \sin 2\beta\ S/N, \tag{97e}$$

$$\gamma_{\phi\epsilon_\times}=\sin\Delta\epsilon\ \cos\theta\ \sin 2\beta\ S/N, \tag{97f}$$

$$\gamma_{\beta\beta}=S/N, \tag{97g}$$

$$\gamma_{\epsilon_+\epsilon_+}=\cos^2\beta\ S/N, \tag{97h}$$

$$\gamma_{\epsilon_\times\epsilon_\times}=\sin^2\beta\ S/N, \tag{97i}$$

where $\Delta\epsilon=\epsilon_\times-\epsilon_+$. Inverting $\boldsymbol{\gamma}$ to find the covariance matrix of simultaneous maximum likelihood estimates of h, θ, ϕ, β, ϵ_+, $\epsilon_\times$ gives the nonzero elements

$$\sigma^2_{hh}=h^2(S/N)^{-1}, \tag{98a}$$

$$\sigma^2_{\theta\theta}=(S/N)^{-1}, \tag{98b}$$

$$\sigma^2_{\phi\phi}=\csc^2\theta(S/N)^{-1}, \tag{98c}$$

$$\sigma^2_{\phi\beta}=2\cos\Delta\epsilon\ \cos\theta\ \csc^2\theta(S/N)^{-1}, \tag{98d}$$

$$\sigma^2_{\phi\epsilon_+}=-2\sin\Delta\epsilon\ \cos\theta\ \csc^2\theta\ \tan\beta(S/N)^{-1}, \tag{98e}$$

$$\sigma^2_{\phi\epsilon_\times}=-2\sin\Delta\epsilon\ \cos\theta\ \csc^2\theta\ \cot\beta(S/N)^{-1}, \tag{98f}$$

$$\sigma^2_{\beta\beta}=(1+4\cos^2\Delta\epsilon\ \cot^2\theta)(S/N)^{-1}, \tag{98g}$$

$$\sigma^2_{\beta\epsilon_+}=-2\sin 2\Delta\epsilon\ \cot^2\theta\ \tan\beta(S/N)^{-1}, \tag{98h}$$

$$\sigma^2_{\beta\epsilon_\times}=-2\sin 2\Delta\epsilon\ \cot^2\theta\ \cot\beta(S/N)^{-1}, \tag{98i}$$

$$\sigma^2_{\epsilon_+\epsilon_+}=(\sec^2\beta+4\sin^2\Delta\epsilon\ \cot^2\theta\ \tan^2\beta)(S/N)^{-1}, \tag{98j}$$

$$\sigma^2_{\epsilon_+\epsilon_\times}=4\sin^2\Delta\epsilon\ \cot^2\theta(S/N)^{-1}, \tag{98k}$$

$$\sigma^2_{\epsilon_\times\epsilon_\times}=(\csc^2\beta+4\sin^2\Delta\epsilon\ \cot^2\theta\ \cot^2\beta)(S/N)^{-1}. \tag{98l}$$

From Eq. (98a), the percentage error in determining the magnitude of the strain spectrum is $\sigma_h/h=(S/N)^{-1/2}$. The maximum likelihood estimates of θ and ϕ are uncorrelated and result in a circular error box on the sky with a mean-square radius covering a solid angle $\Delta\Omega$ given by

$$\Delta\Omega=\pi(\sigma^2_{\theta\theta}+\sin^2\theta\sigma^2_{\phi\phi}) \tag{99a}$$

$$=\frac{2\pi}{(S/N)}. \tag{99b}$$

The results for $\sigma^2_{\theta\theta}$, $\sigma^2_{\phi\phi}$ and $\Delta\Omega$ agree with Zhou and Michelson's analytical and Monte Carlo results [9] despite an apparent factor of 2 discrepancy. Zhou and Michelson used a slightly different definition of S/N based on the optimal receiver for a narrow-band signal of unknown phase. The optimal detection criterion is then to use two optimal filters designed for signal phases 90° apart, and to look for threshold crossings of the sum of the squares of the two filter outputs [23]. In this paper, S/N always denotes the SNR

obtained with the optimal filter when the signal parameters, including phase, are known. This definition gives S/N a value twice that of the Zhou-Michelson definition.

Zhou and Michelson also used Monte Carlo methods to evaluate the uncertainty in measurements of the coordinate independent ''polarization factor'' P defined by

$$P=\sin 2\beta\ \sin\Delta\epsilon. \tag{100}$$

As Zhou and Michelson found, P is a rather nonlinear function, but if the SNR is high enough that only first order terms in $\delta\beta$ and $\delta\Delta\epsilon$ are important, then

$$\delta P\approx\sin 2\beta\ \cos\Delta\epsilon\,\delta\Delta\epsilon+2\cos 2\beta\ \sin\Delta\epsilon\,\delta\beta, \tag{101}$$

and the variance of estimates of P is

$$\sigma_P^2\approx 4\cos^2 2\beta\ \sin^2\Delta\epsilon\,\sigma_\beta^2+\sin^2 2\beta\ \cos^2\Delta\epsilon\,\sigma_{\Delta\epsilon}^2 +4\cos 2\beta\ \sin 2\beta\ \cos\Delta\epsilon\ \sin\Delta\epsilon\,\sigma_{\beta\Delta\epsilon}^2. \tag{102}$$

Using Eqs. (98j) through (98l) to evaluate $\sigma_{\Delta\epsilon}^2=\sigma_{\epsilon_+\epsilon_+}^2+\sigma_{\epsilon_\times\epsilon_\times}^2-2\sigma_{\epsilon_+\epsilon_\times}^2$ and $\sigma_{\beta\Delta\epsilon}^2=\sigma_{\beta\epsilon_\times}^2-\sigma_{\beta\epsilon_+}^2$ gives

$$\sigma_{\Delta\epsilon}^2=4(\csc^2 2\beta+4\cot^2\theta\ \sin^2\Delta\epsilon\ \cot^2 2\beta)(S/N)^{-1}, \tag{103}$$

$$\sigma_{\beta\Delta\epsilon}^2=-4\cot^2\theta\ \sin^2 2\Delta\epsilon\ \cot 2\beta(S/N)^{-1}. \tag{104}$$

Substituting the above into Eq. (102) gives, after simplification, the remarkably simple formula

$$\sigma_P^2\approx 4(1-P^2)(S/N)^{-1}. \tag{105}$$

Actually, Zhou and Michelson measured the absolute value of P and calculated $\sigma_{|P|}^2$ assuming that the source direction is known. If θ and ϕ are known, then the prescription for calculating the estimation covariance matrix is to cross out the rows and columns in $\boldsymbol{\gamma}$ corresponding to θ and ϕ, and then invert the reduced Fisher matrix to find the new covariance matrix. The result is

$$\sigma_{\beta\beta}^2=(S/N)^{-1}, \tag{106a}$$

$$\sigma_{\epsilon_+\epsilon_+}^2=\sec^2\beta(S/N)^{-1}, \tag{106b}$$

$$\sigma_{\epsilon_\times\epsilon_\times}^2=\csc^2\beta(S/N)^{-1}, \tag{106c}$$

with $\sigma_{\beta\epsilon_+}^2=\sigma_{\beta\epsilon_\times}^2=\sigma_{\epsilon_+\epsilon_\times}^2=0$. Substituting into Eq. (102) gives, after simplification, the same simple result as in Eq. (105) calculated for the case of unknown direction. With a spherical antenna, direction accuracy and polarization accuracy are independent.

Comparison with the Zhou-Michelson results is complicated by the effects of measuring $|P|$ instead of P. The difference is most pronounced when P is near zero. Assuming P has an approximately Gaussian probability distribution, the mean and standard deviation of $|P|$ are related to those of P by

$$\langle|P|\rangle=\langle P\rangle\mathrm{erf}\left(\frac{\langle P\rangle}{\sqrt{2}\sigma_P}\right)+\sqrt{\frac{2}{\pi}}\sigma_P\exp\left(\frac{-\langle P\rangle^2}{2\sigma_P^2}\right), \tag{107}$$

$$\sigma_{|P|}^2=\sigma_P^2+\langle P\rangle^2-\langle|P|\rangle^2. \tag{108}$$

The Zhou-Michelson Monte Carlo simulations cover not just very high SNR values, but also low values for which the first-order expansion, Eq. (101), is not valid. Expanding P to second order instead of just first order, and using Eqs. (106a)–(106c) under the assumption of known direction, the mean value $\langle P\rangle$ deviates from the true value according to

$$\langle P\rangle\approx\left(1-\frac{1}{2}\sigma_{\Delta\epsilon}^2-2\sigma_\beta^2\right)P \tag{109}$$

$$=[1-2(\csc^2 2\beta+1)(S/N)^{-1}]P. \tag{110}$$

The deviation of the mean from the true value of P depends not only on the value of P, but also on β. Assuming Zhou and Michelson used $\sin 2\beta=1$ (and varied $\Delta\epsilon$ to change P) reproduces their data well. One final complication needs to be taken into account before comparing this theory with the Zhou-Michelson data: for $P=1$, $2\beta=\Delta\epsilon=\pi/2$ and the first-order terms in the expansion of P are both zero. Thus, for $P=1$, higher order terms must be considered, which gives to leading order

$$\sigma_P^2|_{P=1}\approx 16(S/N)^{-2}. \tag{111}$$

Figures 17 and 18 compare the above analytical expressions for the mean and standard deviation of $|P|$ with the Monte Carlo results in the Zhou-Michelson Fig. 9 [44]. The agreement is excellent for $S/N>60$. The analytical formulas accurately describe both the asymptotic behavior at high SNR and, at intermediate SNR, the effects of the nonlinearity of P and of taking its absolute value.

D. Effect of unequal T_n's on direction accuracy

If a narrow-band lossless spherical detector has radial transducers which do not have identical T_n's, then the detector's direction-finding accuracy becomes anisotropic. In this case, instead of reducing to Eq. (96b), Eq. (94c) for χ becomes (with $\tau=\tau'=0$)

$$\chi(\boldsymbol{\alpha},\boldsymbol{\alpha}')=\mathrm{Re}\left[\mathbf{f}_m^\dagger(\omega_0;\boldsymbol{\alpha})\mathbf{H}^\dagger\int_{-\infty}^{\infty}\frac{d\omega}{2\pi}\mathbf{K}(\omega)\mathbf{H}\mathbf{f}_m(\omega_0;\boldsymbol{\alpha}')\right], \tag{112}$$

where $\mathbf{H}$ is the matrix used to solve Eq. (60) for the effective forces $\mathbf{f}_s$ using the pseudoinverse of $\mathbf{G}^{\mathrm{T}}$ [36]:

$$\mathbf{H}=\sqrt{\frac{5\mu}{4\pi}}(\mathbf{G}^{\mathrm{T}})^+. \tag{113}$$

For a given set of transducer locations and parameters, $\mathbf{H}^\dagger\int_{-\infty}^{\infty}\mathbf{K}d\omega/2\pi\mathbf{H}$ is a constant matrix, which can be evaluated numerically. Then the analytical formulas for $\mathbf{f}_m$ can be differentiated to evaluate Eq. (91) for the Fisher matrix elements.

With identical T_n symmetry, the estimates of θ and ϕ are uncorrelated. When that symmetry is broken, the two direction angles may become correlated and the direction error box changes from a circle to an ellipse with area A given in general by

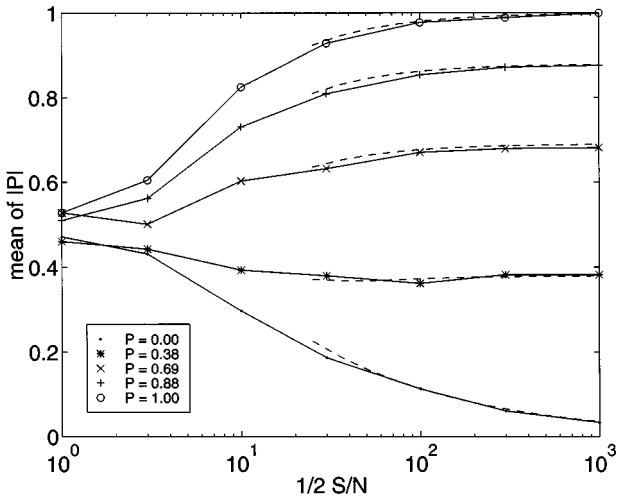

FIG. 17. Mean of the absolute value of the polarization factor. Comparison of the Zhou-Michelson Monte Carlo simulations (points joined by solid lines) and the analytical formulas derived here (dashed curves).

$$A=\pi\sin\theta\sqrt{\sigma_\theta^2\sigma_\phi^2-(\sigma_{\theta\phi}^2)^2}. \tag{114}$$

The effects of broken T_n symmetry were studied numerically for a lossless detector with transducers in the regular dodecahedral locations. As in Sec. V C, a set of six maximally flat single-mode transducer systems was perturbed by changing individual transducer noise temperatures by up to $\pm 20\%$ while holding noise impedances fixed. For any specific source direction and polarization state, the Fisher and covariance matrices were evaluated by the method described above. For circularly polarized signals, the correlation coefficient $\rho_{\theta\phi}=\sigma_{\theta\phi}^2/(\sigma_\theta^2\sigma_\phi^2)^{1/2}$ was found to always be zero, but, for linearly polarized signals, $\rho_{\theta\phi}$ was found to be a sinusoidal function $a\sin 2(\beta-\beta_0)$ with an amplitude dependent on source direction. As before, $T_p^{\rm eff}$ was found to depend on direction and polarization, but for a fixed signal energy,

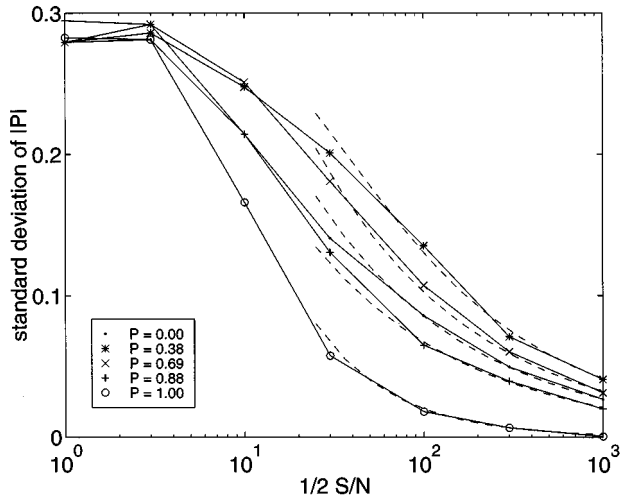

FIG. 18. Standard deviation of maximum likelihood estimates of $|P|$. Comparison of the Zhou-Michelson Monte Carlo simulations (points joined by solid lines) and the analytical formulas derived here (dashed curves).

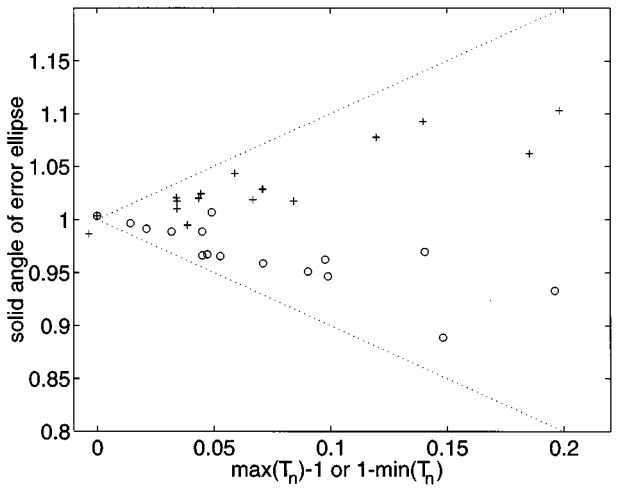

FIG. 19. Solid angle A of the direction error ellipse for lossless spherical detectors with dodecahedrally located transducers but broken T_n symmetry. Units of A are relative to the value for unbroken symmetry. Maximum (+) and minimum (○) values of A over all source directions are plotted versus $\max(T_n)-1$ or $1-\min(T_n)$.

the area A was found to be *completely polarization independent*. However, the area A was less than its identical-T_n value for some directions and larger for others.

Figure 19 shows the size of the anisotropy in A for five random trials at each of the T_n tolerance levels 5, 10, and 20 %. Figure 20 shows maximum value of $|\rho_{\theta\phi}|$ over all directions and polarizations. Empirically, the percentage deviations of A are typically of the same order as, but smaller than, the percentage deviations of T_n. Likewise, $\max(|\rho_{\theta\phi}|)$ shows a first-order effect with values approximately as large as $0.8\times[\max(T_n)-\min(T_n)]/2$.

E. Arrival time estimation

When the arrival time τ is an unknown parameter, Eq. (94c) can be used to calculate the accuracy of arrival time estimates. If the detector has a small fractional bandwidth, then there is trouble distinguishing between arrival time and signal phase. A special case which illustrates this effect most simply is to assume that $\{\theta,\phi,h,\beta,\Delta\epsilon\}$ are known parameters while τ and $\epsilon_0=(\epsilon_+ +\epsilon_\times)/2$ are unknown. The parameter ϵ_0 represents the phase of the true signal wave form relative to its envelope within the detection band. Since $\partial\mathbf{f}_s/\partial\epsilon_0=j\,\mathrm{sgn}(\omega)\mathbf{f}_s$ and $\partial\mathbf{f}_s/\partial\tau=-j\omega\mathbf{f}_s$, it is easy to evaluate the reduced Fisher matrix

$$\gamma_{\epsilon_0\epsilon_0}=(S/N), \tag{115a}$$

$$\gamma_{\epsilon_0\tau}=-\langle\omega\rangle_\alpha(S/N), \tag{115b}$$

$$\gamma_{\tau\tau}=\langle\omega^2\rangle_\alpha(S/N), \tag{115c}$$

where $\langle\omega^n\rangle_\alpha$ is defined by

$$\langle\omega^n\rangle_\alpha=\frac{2\mathrm{Re}[\mathbf{f}_s^\dagger\int_0^\infty(d\omega/2\pi)\omega^n\mathbf{K}(\omega)\mathbf{f}_s]}{2\mathrm{Re}[\mathbf{f}_s^\dagger\int_0^\infty(d\omega/2\pi)\mathbf{K}(\omega)\mathbf{f}_s]}. \tag{116}$$

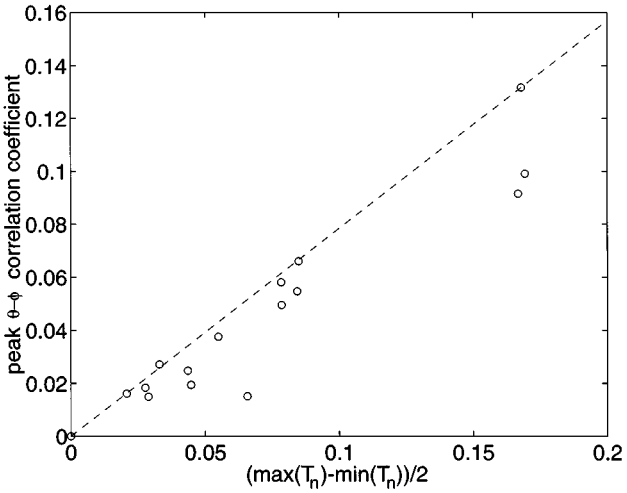

FIG. 20. Correlation coefficient $\rho_{\theta\phi}$ between θ and ϕ estimates for lossless spherical detectors with dodecahedrally located transducers but broken T_n symmetry. Maximum value of $|\rho_{\theta\phi}|$ over all directions and polarizations is plotted versus the fractional spread in noise temperatures.

The value of $\langle\omega^n\rangle_\alpha$ is the nth moment of a probability distribution proportional to the signal-to-noise ratio density for detecting a signal $\mathbf{f}_s(\boldsymbol{\alpha})$. Inverting the Fisher matrix to find the covariance matrix gives

$$\sigma^2_{\epsilon_0\epsilon_0}=\frac{\langle\omega^2\rangle_\alpha}{\langle\omega^2\rangle_\alpha-\langle\omega\rangle^2_\alpha}(S/N)^{-1}, \tag{117a}$$

$$\sigma^2_{\epsilon_0\tau}=\frac{\langle\omega\rangle_\alpha}{\langle\omega^2\rangle_\alpha-\langle\omega\rangle^2_\alpha}(S/N)^{-1}, \tag{117b}$$

$$\sigma^2_{\tau\tau}=\frac{1}{\langle\omega^2\rangle_\alpha-\langle\omega\rangle^2_\alpha}(S/N)^{-1}. \tag{117c}$$

The timing accuracy in Eq. (117c) may be contrasted with the result if ϵ_0 is known in advance:

$$\sigma^2_{\tau\tau}=\frac{1}{\langle\omega^2\rangle_\alpha}(S/N)^{-1}. \tag{118}$$

Thus, if ϵ_0 is not known and the detection bandwidth is narrow, then the uncertainties in estimates of phase and arrival time are highly correlated, and the standard deviation of the arrival time estimate is worse by a factor of $1/\delta^{\rm eff}_\tau$, where $\delta^{\rm eff}_\tau$ is a measure of effective fractional bandwidth defined by

$$\delta^{\rm eff}_\tau=\left(\frac{\langle\omega^2\rangle_\alpha-\langle\omega\rangle^2_\alpha}{\langle\omega^2\rangle_\alpha}\right)^{1/2}. \tag{119}$$

This reproduces a standard result of signal estimation theory for detectors with scalar output [23], but the above calculations show how this applies for a vector detector. The timing accuracy depends on the value of $\delta^{\rm eff}_\tau$ evaluated for a particular source direction and polarization. Although a lossless detector with identical-T_n symmetry was shown above to have isotropic direction and polarization accuracy, its timing accuracy will be anisotropic if the transducers do not exhibit other symmetries which make $\delta^{\rm eff}_\tau$ a constant, such as happens for identical radial transducers in the dodecahedral or icosahedral arrangements, or for the Zhou-Michelson independent transducer design. For the maximally flat, single-mode transducer systems considered in Sec. V, the value of the fractional bandwidth which determines sensitivity to loss has the value $\delta^{\rm eff}=0.148$, while the fractional bandwidth determining timing accuracy is $\delta^{\rm eff}_\tau=0.043$. As the number of modes in a multimode maximally flat transducer system is increased, $\sigma(\omega)$ becomes boxlike and $\delta^{\rm eff}$ approaches the fractional width of the box, while $\delta^{\rm eff}_\tau$ approaches a value $\sqrt{12}$ times smaller. Even for single-mode transducers, the boxlike approximation works well: $\delta^{\rm eff}_\tau$ is only about 10% bigger than $\delta^{\rm eff}/\sqrt{12}$.

If the direction and polarization are not really known, then the full Fisher matrix is more complicated than the reduced matrix given by Eqs. (115a)–(115c). A more detailed analysis of the interplay between direction-polarization and phase-timing uncertainties could be made using the above methods. However, for a narrow-band lossless detector, it was shown above that the direction and polarization uncertainties are of order $(S/N)^{-1}$, which is smaller than the above timing and phase uncertainties by the factor $\delta^{\rm eff}_\tau$. Thus, if $\delta^{\rm eff}_\tau\ll 1$, the direction and polarization are essentially known compared to τ and ϵ_0 and it seems reasonable to assume known direction and polarization when estimating τ and ϵ_0 and calculating their uncertainties.

Although a single narrow-band detector suffers a serious penalty in trying to measure the arrival time of a signal with an unknown shape, the timing accuracy of a network of *identical* detectors is not so bad. With one detector, an error in the value of ϵ_0 used to construct the optimal filter template gives a modest loss of SNR, but a large error in the measured arrival time. However, if groups operating two identical, *similarly oriented*, detectors agree to use arbitrary but equal values of ϵ_0, then even though the arrival times they report will suffer a systematic error, the difference between the measured arrival times will have an uncertainty given approximately by Eq. (118), rather than Eq. (117c). Cerdonio *et al.* [45] have shown that, if the signal shape is assumed known, a global network of 1 kHz bar antennas can have enough timing accuracy according to Eq. (118) to give useful source direction information via time delays starting at modest SNR's of $(S/N)^{1/2}\approx 8$. A network of spherical detectors has the advantage that any two spheres in the network give an accurate time delay, whereas two bars must be aligned to measure the same component of the gravity wave in order for the true signal shape to be the same for each.

VIII. SUMMARY

The approach developed here gives both an intuitive extension to the signal detection and estimation theory for one-dimensional detectors and provides a numerically efficient means of studying the behavior of spherical gravitational wave detectors when various asymmetries exist. Several results were derived which are valid for a general gravitational wave detector employing multiple transducers. Without assuming any particular antenna or transducer symmetries, it was shown that the optimal signal detection algorithm in the

presence of Gaussian noise is unchanged from the scalar detector case: the optimal decision rule for detecting a known signal is always to compute the linear filter *with a scalar output* which maximizes the SNR and to look for the optimal filter output to exceed a threshold. Explicit matrix formulas were derived for computing the optimal linear filter and the resulting SNR in terms of the detector's cross-spectral density matrix and the expected response to the known signal. An explicit construction was given for statistically independent linear combinations of the transducer outputs which simplify the expression for the SNR. The existence of such statistically independent output channels is thus not a consequence of any special symmetries. By introducing admittance matrices which describe the response of the linear detector to signal forces and transducer back-action forces, Price's method [15] of proving Giffard's amplifier limit [13] was generalized to show that, for a lossless detector, the effective pulse detection noise temperature is bounded by the minimum and maximum of the noise temperatures of the individual transducers. If the transducer noise temperatures are identical, then the SNR for detecting an impulsive signal with a lossless detector simply equals E, the energy the signal deposits in an antenna initially at rest, divided by the noise temperature $k_B T_n$ of one transducer. Thus, if the detector is close enough to being lossless, the details of detector design, including the existence of unintended asymmetries, are unimportant since the detector's sensitivity is independent of all other parameters besides E and T_n. If the antenna is also spherical and if there are enough transducers to couple to all the quadrupole modes, the detector's sensitivity is independent of source direction and polarization since E is too. How lossless the detector must be to approach the amplifier limit was shown to depend on the detection bandwidth $\delta^{\rm eff}$ through matrix formulas analogous to those for scalar detectors. Thus for a detector with significant thermal noise to have isotropic sensitivity, an isotropic bandwidth is required in addition to identical T_n's and an isotropic E.

Matrix equations were derived which describe a spherical antenna interacting with a gravitational wave described by general relativity when coupled to N nonidentical, arbitrarily located, multimode transducer systems. If the transducer systems are identical in all respects, then this symmetry was shown to give the equivalence that Johnson and Merkowitz [8] discovered between the SNR spectrum for the spherical detector and a set of bar antennas. It was shown how to evaluate the effective antenna masses of the equivalent bars, and the dodecahedral and icosahedral arrangements were shown to give bandwidth isotropy as a consequence of those arrangements giving the maximal, fivefold, degeneracy of effective masses.

The effects of transducer asymmetries were studied numerically for the dodecahedral design with identical transducers. Location asymmetry was found to leave $T_n^{\rm eff}$ unchanged, but to improve $\delta^{\rm eff}$ for some directions while degrading it for others, giving an anisotropy linear in tolerance and equal to $\pm 10\%$ for $\approx \pm 4^\circ$ tolerance. Tuning asymmetry also leaves $T_n^{\rm eff}$ unchanged, but it always decreases $\delta^{\rm eff}$, little in some directions, and more in others, with a second-order dependence on tolerance. The maximum decrease in $\delta^{\rm eff}$ is limited to 10% for $\approx 5\%$ tolerance. Breaking T_n symmetry while keeping identical noise impedances Z_n leaves $\delta^{\rm eff}$ unchanged, but gives an asymmetry in $T_n^{\rm eff}$ which covers most of the allowed range between $\min(T_n)$ and $\max(T_n)$.

Anisotropy in $T_n^{\rm eff}$ or $\delta^{\rm eff}$ was also used to compare different detector designs and to evaluate their robustness against various transducer failures. Based on its bandwidth anisotropy, the proposed five-transducer arrangement of Lobo and Serrano [20] was found to be inferior to the Johnson-Merkowitz TIGA arrangement of six transducers [8]. The dodecahedral arrangement was found to be fairly robust against excessive additive noise in one transducer; extreme excess noise in one transducer degraded $T_n^{\rm eff}$ by only a factor of 2.4 in the worst case. A regular icosahedral arrangement of ten transducers is more robust against such a transducer failure, but only modestly so. The numerical methods used here could also be used to examine other types of transducer failure, such as one transducer having excess force noise, perhaps because of a poor mechanical Q.

The effects of asymmetries on the accuracy with which a spherical detector can reconstruct source direction, polarization, phase, and arrival time information were studied by generalizing maximum likelihood estimation theory from the scalar to vector case. Deriving formulas for the ambiguity function whose derivatives give the accuracy of the estimates, it was shown that a lossless gravitational wave detector with identical-T_n symmetry looking for impulsive signals has an ambiguity function which is independent of the other transducer parameters. Thus for such a detector, not only is its sensitivity independent of the details of the detector design, but so is the accuracy with which it can reconstruct signal direction and polarization. Consequently, the Zhou-Michelson analysis [9] of direction and polarization accuracy applies not only to their ''independent transducer'' design, but also to any lossless spherical detector with identical-T_n symmetry. The ambiguity function method developed here was shown to reproduce the Zhou-Michelson analytical and Monte Carlo results. The solid angle and polarization factor accuracies were shown to be $\Delta\Omega = 2\pi/(S/N)$ and $\sigma_P^2 = 4(1-P^2)/(S/N)$, the latter formula being an analytical one not derived by Zhou and Michelson. A numerical study of the effects of breaking the T_n symmetry showed that estimates of the direction angles (θ, ϕ) become correlated giving an elliptical rather than circular error box in the sky. For a given source direction, the area of the error box is polarization independent, but the area does depend on the direction, exhibiting an anisotropy first order in the deviations of the noise temperatures. The area is increased in some directions and decreased in others by fractional amounts almost as large as the fractional changes in the maximum and minimum T_n. The peak θ–ϕ correlation coefficient is as large as $0.8\times[\max(T_n)-\min(T_n)]/2$. The accuracy of arrival time estimates was shown to depend on the detection bandwidth, so asymmetries which give bandwidth anisotropy will also give an arrival time uncertainty which varies in inverse proportion to the bandwidth.

While the analysis presented here has not exhaustively covered the effects of all possible detector asymmetries, some of the results are general enough to show that both the sensitivity and the signal reconstruction abilities of a spherical gravitational wave detector are reasonably immune to

even fairly large asymmetries, provided care is taken to experimentally characterize the detector's noise and its response to signal so that the required optimal filters may be constructed. One of the theoretical questions which remain is how best to determine, in a practical way, the expected response to the bulk forces of a gravitational wave when only surface forces can be applied to the antenna for calibration in the laboratory. However, the detector characterization is done, the matrix formulas derived here for the optimal linear filters should prove useful when the day comes for such detectors to begin observing the gravitational sky.

ACKNOWLEDGMENTS

I would like to thank H. J. Paik and G. M. Harry for extensive comments and criticism. I also thank C. Zhou and S. M. Merkowitz for helpful discussions regarding their work. This work was supported under NSF Grant No. PHY-93-12229.

[1] An American collaboration among researchers at the University of Maryland, Louisiana State University, the University of Rochester, and Santa Clara University has been formed to design and build spherical antennas. There are also collaborations in Italy, the Netherlands, and Brazil.
[2] A. Abramovici *et al.*, Science **256**, 325 (1992).
[3] C. Bradaschia *et al.*, Nucl. Instrum. Methods Phys. Res. A **289**, 518 (1990), B. Caron *et al.*, *ibid.* **360**, 258 (1995).
[4] K. Danzmann *et al.*, in *Relativistic Gravity Research*, Proceedings of the 81st W. E. Heraeus Seminar, Bad Honnef, Germany, edited by J. Ehlers and G. Schäfer (Springer-Verlag, Berlin, 1992).
[5] R. L. Forward, Phys. Rev. D **2**, 149 (1971).
[6] N. Ashby and J. Dreitlein, Phys. Rev. D **12**, 336 (1975).
[7] R. V. Wagoner and H. J. Paik, *Experimental Gravitation*, Proceedings of the Pavia International Symposium, Pavia, Italy (Academia Nazionale dei Lincei, Rome, 1977).
[8] W. W. Johnson and S. M. Merkowitz, Phys. Rev. Lett. **70**, 2367 (1993).
[9] C. Zhou and P. F. Michelson, Phys. Rev. D **51**, 2517 (1995); Z. Zhou, Ph.D. thesis, Stanford University, 1994.
[10] E. Coccia and V. Fafone, Phys. Lett. A **213**, 16 (1996).
[11] G. M. Harry, T. R. Stevenson, and H. J. Paik, Phys. Rev. D **54**, 2409 (1996).
[12] S. M. Merkowitz and W. W. Johnson, Phys. Rev. D **51**, 2546 (1995).
[13] R. P. Giffard, Phys. Rev. D **14**, 2478 (1976).
[14] P. F. Michelson and R. C. Taber, Phys. Rev. D **29**, 2149 (1984).
[15] J. C. Price, Phys. Rev. D **36**, 3555 (1987).
[16] T. R. Stevenson, in *First Edoardo Amaldi Conference on Gravitational Wave Experiments*, Frascati, Italy, 1994, edited by E. Coccia, G. Pizzella, and F. Ronga (World Scientific, Singapore, 1995), p. 455.
[17] T. R. Stevenson, in *Proceedings of OMNI-1, First International Workshop for an Omnidirectional Gravitational Radiation Observatory*, São José dos Campos, Brazil, 1996, edited by O. Aguiar and W. Velloso (World Scientific, Singapore, 1997).
[18] S. M. Merkowitz, Ph.D. thesis, Louisiana State University, 1995.
[19] S. M. Merkowitz and W. W. Johnson, Phys. Rev. D **53**, 5377 (1996).
[20] J. A. Lobo and M. A. Serrano, Europhys. Lett. **35**, 253 (1996).
[21] C. H. Cook and M. Bernfeld, *Radar Signals, an Introduction to Theory and Application* (Artech House, Boston, 1993) [originally published by Academic, New York, 1967, 1987].
[22] *Detection and Estimation: Applications to Radar*, edited by S. S. Haykin (Dowden, Hutchington and Ross, Stroudsburg, 1976).
[23] A. D. Whalen, *Detection of Signals in Noise* (Academic, New York, 1971).
[24] D. O. North, Proc. IEEE **51**, 1016 (1963), reprinted with editorial comments in [22].
[25] L. A. Wainstein and V. D. Zubakov, *Extraction of Signals from Noise* (Prentice-Hall International, London, 1962).
[26] V. B. Braginsky, in *Topics in Theoretical and Experimental Gravitation Physics*, Proceedings of the International School of Cosmology and Gravitation, Erice, Sicily, 1975, edited by V. De Sabbata and J. Weber (Plenum, London, 1977), p. 105; V. B. Braginsky and Yu. I. Vorontsov, Sov. Phys. Usp. **17**, 644 (1975); V. B. Braginsky, Yu. I. Vorontsov, and V. D. Krivchenkov, Sov. Phys. JETP **41**, 28 (1975).
[27] H. Heffner, Proc. IRE **50**, 1604 (1962), but note Heffner uses a slightly different definition for T_n.
[28] H. J. Paik, J. Appl. Phys. **47**, 1168 (1976).
[29] J. A. Lobo, Phys. Rev. D **52**, 591 (1995).
[30] E. Coccia, J. A. Lobo, and J. A. Ortega, Phys. Rev. D **52**, 3735 (1995).
[31] A. E. H. Love, *A Treatise on the Mathematical Theory of Elasticity* (Dover, New York, 1944).
[32] J.-P. Richard, in *Proceedings of the Second Marcel Grossmann Meeting on General Relativity*, Trieste, 1979, edited by R. Ruffini (North-Holland, Amsterdam, 1982); Phys. Rev. Lett. **52**, 165 (1984).
[33] See [15], Eq. (34), for example.
[34] J. B. Johnson, Phys. Rev. **32**, 97 (1928); H. Nyquist, *ibid.* **32**, 110 (1928); H. B. Callen and T. A. Welton, *ibid.* **83**, 34 (1951).
[35] **M** is not invertible for $N \geqslant 6$ but has the same null space as $\mathbf{Y}_{ts}$, so Eq. (53) makes sense. Using the pseudoinverse $\mathbf{M}^{+}$ avoids difficulties [36].
[36] G. Strang, *Linear Algebra and its Applications* (Academic, New York, 1976), Chap. 3.
[37] MATLAB, The MathWorks, Inc., 24 Prime Way, Natick, MA 01760.
[38] Figures 1 and 2 show the maximum and minimum of δ^{eff} over all general, elliptical, polarization states, but analysis of Eqs. (59) and (68) shows that, with identical T_n's, the extremal values of δ^{eff} are attained for linearly polarized signals.
[39] N. S. Magalhães *et al.*, Mon. Not. R. Astron. Soc. **274**, 670 (1995).

[40] H. Cramer, *Mathematical Methods of Statistics* (Princeton University Press, Princeton, NJ, 1958); see also Sec. (10.5) of [23].

[41] N. Wiener, Acta Math. **55**, 117 (1930); and later, independently, A. Khintchine, Math. Ann. **19**, 604 (1934); also, G. I. Taylor, Proc. London Math. Soc. Sec. 2, **20**, 196 (1920); Proc. R. Soc. London **164**, 476 (1938).

[42] See [21], Chap. 4.

[43] MATHEMATICA, Wolfram Research, Inc., 100 Trade Center Drive, Champaign, IL 61820.

[44] Note that the ordinate of Fig. 9(b) in the Zhou-Michelson paper [9] is mislabeled as variance when it is actually standard deviation.

[45] M. Cerdonio *et al.*, Phys. Rev. Lett. **71**, 4107 (1993).